HHS Public Access

Author manuscript

Nat Cell Biol. Author manuscript; available in PMC 2016 July 01.

Published in final edited form as:

Nat Cell Biol. 2016 January ; 18(1): 7–20. doi:10.1038/ncb3280.

Sequential Notch activation regulates ventricular chamber development

Gaetano D'Amato[1], **Guillermo Luxán**[1], **Gonzalo del Monte-Nieto**[1], **Beatriz Martínez-Poveda**[1], **Carlos Torroja**[2], **Wencke Walter**[2], **Matthew S. Bochter**[3], **Rui Benedito**[4], **Susan Cole**[3], **Fernando Martinez**[2], **Anna-Katerina Hadjantonakis**[5], **Akiyoshi Uemura**[6], **Luis J. Jiménez-Borreguero**[7,8], and **José Luis de la Pompa**[1,9]

[1]Intercellular Signalling in Cardiovascular Development & Disease Laboratory, Centro Nacional de Investigaciones Cardiovasculares (CNIC), Melchor Fernández Almagro 3, 28029 Madrid, Spain.

[2]Bioinformatics Unit, CNIC, Melchor Fernández Almagro 3, 28029 Madrid, Spain.

[3]Department of Molecular Genetics, Ohio State University, Columbus, Ohio 43210, USA.

[4]Molecular Genetics of Angiogenesis Laboratory, CNIC, Melchor Fernández Almagro 3, 28029 Madrid, Spain.

[5]Developmental Biology Program, Sloan-Kettering Institute, New York, New York 10065, USA.

[6]Department of Retinal Vascular Biology, Nagoya City University Graduate School of Medical Sciences, 1 Kawasumi Mizuho-cho, Mizuho-ku, Nagoya 467-8601, Japan.

[7]Cardiovascular Imaging Laboratory, CNIC, Melchor Fernández Almagro 3, 28029 Madrid, Spain.

[8]Instituto de Investigación Sanitaria Hospital La Princesa, 28006 Madrid, Spain.

Abstract

Ventricular chambers are essential for the rhythmic contraction and relaxation occurring in every heartbeat throughout life. Congenital abnormalities in ventricular chamber formation cause severe human heart defects. How the early trabecular meshwork of myocardial fibres forms and subsequently develops into mature chambers is poorly understood. We show that Notch signalling first connects chamber endocardium and myocardium to sustain trabeculation, and later coordinates ventricular patterning and compaction with coronary vessel development to generate the mature chamber, through a temporal sequence of ligand signalling determined by the

[9]Correspondence should be addressed to J.L.d.l.P. (jlpompa@cnic.es).

METHODS

Methods and any associated references are available in the online version of the paper.

Note: Supplementary Information is available in the online version of the paper

AUTHOR CONTRIBUTIONS

G.D'A., G.L., G.d.M.-N., B.M.-P. and M.S.B. performed experiments. C.T., W.W. and F.M. analysed the RNA-seq data, A.-K.H., A.U. and S.C. provided the *CBF:H2B-Venus* reporter, the *MFng* transgenic line and the $M^{-/-};L^{-/-};R^{-/-}$ embryos. R.B. advised on the Fng experiments and L.J.J.-B. evaluated ultrasonography and CMRI. J.L.d.l.P. designed experiments, reviewed the data and wrote the manuscript. All authors reviewed the manuscript.

COMPETING FINANCIAL INTERESTS

The authors declare no competing financial interests.

glycosyltransferase manic fringe (MFng). Early endocardial expression of MFng promotes Dll4–Notch1 signalling, which induces trabeculation in the developing ventricle. Ventricular maturation and compaction require MFng and Dll4 downregulation in the endocardium, which allows myocardial Jag1 and Jag2 signalling to Notch1 in this tissue. Perturbation of this signalling equilibrium severely disrupts heart chamber formation. Our results open a new research avenue into the pathogenesis of cardiomyopathies.

Ventricular chamber development begins with the formation of trabeculae, a mesh of endocardium-lined luminal cardiomyocyte projections[1,2]. Trabeculae extend radially and longitudinally, forming a network that comprises most of the myocardial mass, increasing myocardial surface area for gas exchange[1]. Subsequent remodelling and compaction thickens the trabeculae radially until they are indistinguishable from the myocardial wall. Simultaneously, epicardium-derived cells[3] invade the outer compact myocardium and together with ventricular endocardial cells[4] contribute to the coronary vasculature that will support the final growth phase and nourish the adult myocardium[5]. Defective trabecular compaction manifests as left ventricular non-compaction (LVNC) cardiomyopathy, characterized by prominent trabeculations separated by deep intertrabecular recesses in a thin ventricular wall[6,7]. LVNC is a genetic cardiomyopathy[8] caused by mutations in genes encoding sarcomeric, cytoskeletal and nuclear-membrane proteins, and can manifest as depressed systolic function or as serious complications including systemic embolism, malignant arrhythmias, heart failure and sudden death[9,10]. LVNC is generally transmitted as an autosomal dominant trait, but the underlying disease mechanisms are poorly understood[7,11].

Inactivation of the Notch1 receptor or its effector RBPJK disrupts trabeculation owing to impaired trabecular endocardium and myocardium differentiation and reduced ventricular cardiomyocyte proliferation[12]. Moreover, targeted inactivation of the Notch pathway modulator mind bomb1 (Mib1) in murine myocardium disrupts ventricular chamber maturation leading to LVNC. Mib1 is an E3-ubiquitin ligase that ubiquitylates Notch ligands, triggering their endocytosis and the transendocytosis of the Notch extracellular domain[13], this last event being essential for generation and release of the Notch intracellular domain[14] (NICD). Inactivating mutations in human *MIB1* have been identified in patients with autosomal dominant familial LVNC (ref. 15). Thus, the NOTCH pathway plays central roles in ventricular chamber development and LVNC (refs 12,15), but the signalling elements and underlying regulatory circuitries involved are unresolved.

Endocardial Dll4 and myocardial Jag1 are candidate Notch ligands in the early mouse heart

Using the single-cell-resolution Notch reporter line *CBF:H2B-Venus* (ref. 16), we mapped Notch activation in the developing ventricles in relation to the ligands Dll4 and Jag1. *CBF:H2B-Venus* was widely expressed in chamber endocardium of embryonic day 9.5 (E9.5) wild-type (WT) *CBF:H2B-Venus* embryos, and expression was abrogated in *RBPJk*- and *Notch1*-targeted mutants (Fig. 1a and Supplementary Fig. 1a). Whole-mount staining of E9.5 *CBF:H2B-Venus* hearts for α-smooth-muscle actin (SMA) and CD31, also known as

Pecam1, confirmed endocardial Notch activity (Fig. 1b,b′ and Supplementary Video 1). At E9.5, Dll4 was preferentially expressed in the endocardium at the base of developing trabeculae, while Jag1 was expressed in trabecular myocardium, both coinciding with sites of *CBF:H2B-Venus* activity (Fig. 1c–d′). Amira-3D reconstructions of the early expression patterns of Dll4 (Supplementary Fig. 1b and Supplementary Data File 1), Jag1 (Supplementary Fig. 1b and Supplementary Data File 2) and N1ICD (Supplementary Fig. 1b and Supplementary Data File 3 and refs 12,15) supported these observations. Endocardial *Dll4* expression weakened from E12.5 to E15.5 (Supplementary Fig. 1c,c′) and *Dll4* transcription disappeared by E15.5 but persisted in coronary vessel endothelium (Supplementary Fig. 1e,e′). In contrast, Jag1 expression expanded to the compact myocardium but was weaker than in trabeculae and coronary vessels (Supplementary Fig. 1d,d′,f,f′,h,h′) whereas Notch activity was detected throughout endocardium and coronary vessel endothelium (Supplementary Fig. 1g,h′).

Dll4–Notch1 signalling inactivation disrupts trabeculation and coronary vessel formation

We next crossed mice bearing a conditional $Dll4^{flox}$ allele[17] with the pan-endothelial and pan-endocardial driver lines *Tie2-Cre* (ref. 18) and *Nfatc1pan-Cre* (ref. 4). $Dll4^{flox}$ inactivation with either driver severely disrupted trabeculation (Fig. 1e–g′) producing a phenotype similar to that of *Notch1* inactivation (Fig. 1h,h′). At E9.5, myosin (MF20) and CD31/Pecam1 staining of mutant hearts revealed reductions in compact myocardium thickness (28%) and trabecular length (50%; Fig. 1i). N1ICD expression was below normal in the ventricular endocardium of E9.5 $Dll4^{flox}$*;Nfatc1pan-Cre* and $Dll4^{flox}$*;Tie2-Cre* mutants (Supplementary Fig. 2a,b). In $Dll4^{flox}$*;Tie2-Cre* mutants, *Hey2* transcription marked a thin compact myocardium and was reduced in the endocardium (Supplementary Fig. 2c). Mutant embryos also showed reduced *EfnB2*, *Nrg1* and *Bmp10* transcription (Supplementary Fig. 2c), known to depend on Notch activity[12].

To determine the role of cardiac Dll4 at later stages, we bred $Dll4^{flox}$ mice with the driver $Cdh5\text{-}Cre^{ERT}$, active in endocardium and vascular and coronary vessel endothelium[19]. At E15.5, $Dll4^{flox}$;$Cdh5\text{-}Cre^{ERT}$ embryos had neck oedema, suggesting circulatory problems (Supplementary Fig. 3a,c). Ventricular wall thickness was reduced in $Dll4^{flox}$;$Cdh5\text{-}Cre^{ERT}$ mutants (Supplementary Fig. 3b,d). *Dll4*, strongly expressed in WT coronary vasculature (Supplementary Fig. 3e,e′), was markedly reduced in mutants (Supplementary Fig. 3f,f′). N1ICD was still expressed in $Dll4^{flox}$;$Cdh5\text{-}Cre^{ERT}$ chamber endocardium but was almost absent in intramyocardial coronary vessels (Supplementary Fig. 3g,h′). $Dll4^{flox}$;$Cdh5\text{-}Cre^{ERT}$ mutant hearts showed normal *Hey2* expression in compact myocardium (Supplementary Fig. 3i,j′) but the coronary artery endothelial markers *HeyL*, *EfnB2* and *Cx40*, also known as *Gja5*, (Supplementary Fig. 3k–p′) were downregulated.

Cardiac Dll4–Notch1 gene profiling

To identify Notch targets, we profiled E9.5 WT, $Dll4^{flox}$*;Tie2-Cre*, $Dll4^{flox}$*;Nfatc1pan-Cre* and $Notch1^{flox}$*;Nfatc1pan-Cre* hearts by RNA sequencing (RNA-seq). $Dll4^{flox}$*;Tie2-Cre* mutants showed 2,101 affected genes (1,179 upregulated, 922 downregulated),

Dll4^{flox}*;Nfatc1pan-Cre* mutants 1,321 (916 upregulated, 405 downregulated) and *Notch1*^{flox}*;Nfatc1pan-Cre* mutants 631 (472 upregulated, 159 downregulated; P <0.05; Fig. 1j and Supplementary Table 1). The three mutants shared 142 differentially expressed genes (Supplementary Table 1). *Dll4*^{flox}*;Tie2-Cre* and *Dll4*^{flox}*;Nfatc1pan-Cre* mutants shared 702 genes, *Dll4*^{flox}*;Tie2-Cre* and *Notch1*^{flox}*;Nfatc1pan-Cre* mutants 238, and *Notch1*^{flox}*;Nfatc1pan-Cre* and *Dll4*^{flox}*;Nfatc1pan-Cre* mutants 202 (Fig. 1k). Gene ontology (GO) classification revealed deregulation of genes involved in cardiovascular development and disease, cell cycle and proliferation, cell death, dilated cardiomyopathy and intercellular pathways (Fig. 1l and Supplementary Fig. 4a,b). *Dll4*^{flox}*;Tie2-Cre* and *Dll4*^{flox}*;Nfatc1pan-Cre* mutants showed upregulation of the negative regulators of cellular proliferation *Cdkn1a* (also known as *p21*), *Cdkn1b*, *Gadd45a*, *Foxo3*, *Cbx7*, *Ccng2*, *Ndrg1*, *Myct1* and *Runx1* (Fig. 1l). Consistently, cardiomyocyte proliferation was 42% lower in *Dll4*^{flox}*;Nfatc1pan-Cre* mutants than in WT counterparts (Fig. 1m–o).

The three genotypes showed pronounced downregulation of *Gpr126* (Fig. 1l and Supplementary Table 1), encoding an orphan adhesion G protein-coupled receptor[20] whose inactivation in mice causes hypotrabeculation and ventricular wall thinning[21,22]. *Gpr126* was transcribed in E9.5 WT endocardium and downregulated in *Dll4*^{flox}*;Nfatc1pan-Cre* mutants (Fig. 1p–q′). Cardiac expression of zebrafish *gpr126* was abrogated in Notch-deficient *mib1*^{ta52b} mutant larvae (Supplementary Fig. 2d,e′) and in WT larvae treated with the Notch inhibitor RO4929097 (ref. 23; Supplementary Fig. 2d,d′,f,f′). Endocardial *Gpr126* expression, the trabecular phenotype of *Gpr126* mutant mice[21,22], and *Gpr126* downregulation in mouse and zebrafish Notch mutants suggest that it as a Notch target during trabeculation. To substantiate the relationship between Notch and *Gpr126*, we conducted real-time quantitative PCR with reverse transcription (qRT–PCR) on Dll4-stimulated HUVEC. Dll4 increased *Gpr126* expression, an effect abolished by RO4929097 (Supplementary Fig. 2g). *In silico* analysis revealed two conserved putative RBPJK-binding sites in *Gpr126* intron four. Luciferase reporter assays in bovine aortic endothelial cells (BAEC) showed that increasing amounts of N1ICD were able to transiently activate the *Gpr126* reporter fivefold (Supplementary Fig. 2h).

Adult heart function requires signalling from myocardial Jag1 to endocardial Notch1

Jag1 inactivation with the early myocardial driver *cTnT-Cre* (ref. 24) did not affect trabeculation (Supplementary Fig. 5a); moreover, despite efficient deletion of *Jag1*^{flox} in the ventricles, N1ICD expression was unaffected in E10.5 *Jag1*^{flox}*;cTnT-Cre* mice (Supplementary Fig. 5a,b). Similarly, expression of *Hey2*, *EfnB2*, *Nrg1* and *Bmp10* seemed normal (Supplementary Fig. 5c). Jag1 thus seems not to be required for trabeculation and Notch1 activation in the early ventricle. In E13.5 *Jag1*^{flox}*;cTnT-Cre* embryos, myocardial Jag1 expression is abrogated and endocardial N1ICD expression is markedly reduced (Supplementary Fig. 5d), indicating that at this stage Notch1 activity in the ventricles depends on Jag1 signalling.

E16.5 WT embryos had a thick compact myocardium and compacting trabeculae, whereas *Jag1*^{flox}*;cTnT-Cre* embryos revealed a 21% thinner compact myocardium in the right

ventricle (Fig. 2a–b′,g). Mutant embryos also showed 30% and 42% higher trabecular complexity in the left and right ventricles (Fig. 2g). Increased trabecular complexity is a hallmark of LVNC and hypertrophic cardiomyopathies[25]. WT neonates had thick muscular ventricular walls (Fig. 2c,c′), but *Jag1^{flox};cTnT-Cre* littermates had dilated ventricles and a thin compact myocardium (Fig. 2d,d′). These defects were also apparent in mutant adult heart (Fig. 2e–f′). Ultrasonography revealed impaired left ventricular systolic function in adult *Jag1^{flox};cTnT-Cre* mutants, with reductions in ejection fraction, fractional shortening and diastolic interventricular septal wall thickness (Fig. 2h,i and Supplementary Video 2). High-resolution cardiac magnetic resonance imaging (CMRI) confirmed ventricular wall thinning in *Jag1^{flox};cTnT-Cre* animals (Fig. 2h and Supplementary Video 3). CMRI also revealed reductions in left ventricular ejection fraction, cardiac output, end-systolic mass, end-diastolic volume and the thickness of right ventricular free wall (Fig. 2j), which also showed segmental dyskinesia (Supplementary Video 4).

Jag1 is required for ventricular maturation

Chamber marker analysis in E16.5 *Jag1^{flox};cTnT-Cre* embryos revealed expansion of the compact myocardium marker *Hey2* to the trabeculae (Fig. 2k–l′) and low expression of the trabecular markers *Bmp10*, *Gja5/Cx40* (Fig. 2m–p′) and *Anf* (Supplementary Fig. 5e,f′), especially in the right ventricle.

RNA-seq of E15.5 *Jag1^{flox};cTnT-Cre* ventricles identified 97 differentially expressed genes ($P < 0.05$): 74 upregulated, 23 downregulated (Fig. 3a and Supplementary Table 1). GO classification revealed involvement in essential cellular functions, cardiovascular development and disease, and dilated cardiomyopathy (Fig. 3b). E16.5 *Jag1^{flox};cTnT-Cre* mutants showed strong downregulation of the chemokine ligand gene *Cxcl12* (Fig. 3b,c and Supplementary Table 1), with attenuated chamber myocardium expression at E16.5 (Fig. 3d–e′). Interestingly, Cxcl12/Cxcr4 signalling is crucial for coronary artery development[26,27], a process simultaneous with and essential for compaction[28]. One upregulated gene was the cell-cycle inhibitor *Cdkn1a/p21* (Fig. 3b and Supplementary Table 1). Consistent with RNA-seq, p21 expression was 30% above normal in E13.5 *Jag1^{flox};cTnT-Cre* mutant ventricles (Fig. 3f–g′,n) concomitantly with reductions in compact myocardium proliferation (56%) and endocardial N1ICD expression (28%; Fig. 3h–i′,n). This defect persisted at E16.5 when *Jag1^{flox};cTnT-Cre* embryos had a 25% below-normal proliferation of compact myocardium cardiomyocytes (Fig. 3j–k′,n). *In situ* hybridization (ISH) and qRT–PCR in E16.5 *Jag1^{flox};cTnT-Cre* mutants revealed reduced *Gpr126* transcription (Fig. 3c,l–m′), similar to the situation in *Dll4* mutants (Fig. 1p–q′).

Jag2 is required for chamber maturation and compaction together with Jag1

Targeted *Mib1* inactivation in mouse myocardium causes LVNC cardiomyopathy[15]. We expected similar cardiac phenotypes in *Mib1^{flox};cTnT-Cre* and *Jag1^{flox};cTnT-Cre* mutants, assuming Jag1 as the only myocardial ligand and therefore the only potential Mib1 substrate. This was not the case: E16.5 *Jag1^{flox};cTnT-Cre* mutants showed a thin compact myocardium and altered ventricular patterning, and adult mutants showed structural and

functional signs of cardiomyopathy and systolic dysfunction, but not LVNC (Fig. 2). The phenotypic differences between *Mib1* and *Jag1* mutants suggested that another Notch ligand might be acting in the myocardium.

Myocardial expression of *Jag2*, a mammalian *Jag1* paralogue, was upregulated from E10.5, (Fig. 4a). *Jag2* upregulation paralleled *Jag1* downregulation so that at E12.5–14.5 *Jag1* and *Jag2* expression levels were similar, with *Jag2* levels higher thereafter (Fig. 4a). E16.5 $Jag2^{flox}$;*cTnT-Cre* mice showed strongly diminished *Jag2* expression in myocardium (Fig. 4a), and had a poorly structured ventricular septum and a 38% thinner compact myocardium, paralleled by a 20% increase in trabecular complexity (Fig. 4b–c′,e). Compact myocardium thinning was most likely due to the 30% reduced cardiomyocyte proliferation at E13.5, especially in the right ventricle (Fig. 4f,g,l). Consistent with action of Jag2 as a cardiac Notch ligand, N1ICD expression was 35% reduced in the right ventricle of E16.5 $Jag2^{flox}$;*cTnT-Cre* embryos (Fig. 4i,j,l), indicating that myocardial *Jag2* deletion disrupted endocardial Notch activation. Furthermore, *Hey2*, *Bmp10* and *Gpr126* were downregulated in $Jag2^{flox}$;*cTnT-Cre* mutants (Fig. 4m–r).

We next generated mice doubly deficient for myocardial *Jag1* and *Jag2*. E16.5 $Jag1^{flox}$;$Jag2^{flox}$;*cTnT-Cre* embryos have a very thin compact myocardium, especially the ventricular apex region (Fig. 4d,d′), with a 27% thinner compact myocardium overall (Fig. 4e and Supplementary Fig. 6a). In contrast, trabecular complexity and trabecular area were respectively 26% and 72% above normal in the right ventricle of $Jag1^{flox}$;$Jag2^{flox}$;*cTnT-Cre* mice (Fig. 4e and Supplementary Fig. 6a), indicating defective compaction. Immunostaining of E16.5 $Jag1^{flox}$;$Jag2^{flox}$;*cTnT-Cre* heart sections for cTnT and endomucin, to label the myocardium and endocardium, showed a severe chamber phenotype (Supplementary Fig. 7a–b″), reminiscent of $Mib1^{flox}$;*cTnT-Cre* mice[15]. Cardiomyocyte proliferation in E13.5 $Jag1^{flox}$;$Jag2^{flox}$;*cTnT-Cre* compact myocardium was 40% below normal in both ventricles (Fig. 4f,h,l). Endocardial Notch1 activity was also significantly reduced (32%, Fig. 4i,k,l). *Hey2* delineated a thin compact myocardium with deep recesses (see below), *Bmp10* was expressed in the trabeculae and endocardial *Gpr126* expression was attenuated (Fig. 4m–o,s–u). Jag1 and Jag2 thus seem to play non-redundant roles in chamber development.

Manic Fringe modulates Notch ligand selectivity in ventricular endocardial cells

The Fringe family of glycosyltransferases elongate carbohydrates attached to the Notch extracellular EGF-like repeats, contributing to ligand selectivity[29]. On Notch glycosylation, Delta-Notch signalling is enhanced, and Jag/Ser–Notch signalling is diminished[29,30]. We first examined embryonic cardiac expression of the three mammalian Fringe paralogues by ISH and qRT–PCR. *Manic fringe* (*MFng*) was transcribed in chamber endocardium from E8.5, subsequently declining to a minimum at E11.5 (Fig. 5a,b). In contrast, *lunatic fringe* (*LFng*) was transcribed in epicardium and *radical fringe (RFng)* was not detected in the heart (Supplementary Fig. 8a,b). ISH data for *MFng* suggested that MFng activity in E8.5–10.5 chamber endocardium would favour endocardial Dll4 signalling to the Fringe-modified Notch receptor.

We investigated the effect of MFng on ligand stimulation of Notch1, using isolated and immortalized mouse embryonic ventricular endocardial cells (MEVEC) transduced with lentiviral vector encoding MFng (*MFng*-MEVEC). We first examined the response of control *GFP*–MEVEC to stimulation with immobilized recombinant Dll4, Jag1 or Jag2 ligands[31]. As readouts we measured the activity of the Notch reporter CBF1–Luc (ref. 32; Fig. 5c) and transcript expression of endocardial Notch target *Hey1* (ref. 33; Fig. 5d). Dll4 and Jag1 activated the Notch reporter to a similar extent, whereas Jag2 elicited a weaker response (Fig. 5c), but all three ligands induced a similar increase in *Hey1* expression (Fig. 5d). Pairwise ligand combinations produced additive effects (Fig. 5c). In *MFng*-MEVEC Notch reporter activity and *Hey1* expression were potentiated by Dll4, whereas the response to Jag1 and Jag2 remained weak (Fig. 5c,d). Combinations of Dll4+Jag1 and Dll4+Jag2 produced a similar response to stimulation with Dll4 alone (Fig. 5c,d), but the Jag1+Jag2 combination stimulated Notch signalling weakly (Fig. 5c,d).

Systemic *Fng* inactivation affects coronary vessel development

Our data suggest that MFng may regulate the spatio-temporal specificity of Notch ligand–receptor interaction in the developing chamber. In E8.5–10.5 chamber endocardium, MFng would favour endocardial Dll4 signalling to the Fringe-modified Notch receptor. *MFng* downregulation after E11.5 would allow Jag1 and Jag2 myocardial signalling to activate endocardial Notch1. We examined the effect of systemic *Fng* inactivation by generating mice triply deficient for *M*, *L* and *RFng*. Triple mutants develop to term and, although not found at Mendelian frequency at weaning, there are no reported embryonic lethal phenotypes[34]. Examination of *M;L;RFng*-deficient embryos at E10.5 revealed no obvious trabeculation defects, suggesting that Dll4 (and Jag1) is able to activate Notch signalling sufficiently. At E16.5, WT chamber development is well advanced (Fig. 5e,e′) and $M^{-/-};L^{-/-};R^{-/-}$ embryos had a 33% thinner compact myocardium (Fig. 5f,f′,k); moreover, CD31 staining revealed coronary vessel loss or defects (Fig. 5g,h). Interestingly, N1ICD expression seemed normal in ventricular endocardium but was attenuated in coronary vessels (Fig. 5i–j′). *Hey2* expression marked the thin compact myocardium and *Cx40* was expressed in trabeculae but did not label coronary vessels in $M^{-/-};L^{-/-};R^{-/-}$ mice (Fig. 5l). Coronary arteries of E16.5 *Fng*-deficient embryos also showed abnormal expression patterns of *Dll4*, *Hey1*, *HeyL* and *EfnB2* (Fig. 5m), similar to E15.5 $Dll4^{flox};Cdh5\text{-}Cre^{ERT}$ mutant hearts (Supplementary Fig. 3k–p′). Systemic *Fng* abrogation disrupts coronary vessel development, crucial for myocardium nourishment, thus indirectly affecting compaction. During compaction *MFng* is expressed in coronary vessels (Fig. 6a), similarly to *Dll4* (Supplementary Figs 1e,e′ and 3e,e′) suggesting that MFng may reinforce Dll4 signalling to Notch in the developing coronaries.

Forced *MFng* expression disrupts chamber development and compaction

Our *in vitro* data predicted that forced endocardial MFng expression would hamper Jag1- and Jag2-mediated Notch1 activation, producing a chamber phenotype similar to that caused by inactivation of both ligands (Fig. 4d,d′ and Supplementary Fig. 7b–b″) or *Mib1* inactivation (Supplementary Fig. 7d–d″ and ref. 15). We generated a transgenic line ($MFng^{tg}$) bearing a *Rosa26-CAG-floxNeoSTOPflox-MFng-EGFP* expression cassette (Fig.

6b). *Tie2-Cre*-mediated[18] removal of the *NeoSTOP* sequences resulted in *Rosa26-CAG*-driven *MFng-EGFP* expression in vascular endothelium and endocardium (Fig. 6b,c,c′). At E16.5, transgenic mice with two *MFng–EGFP* copies had a dilated heart, with compact myocardium 50–60% thinner than WT (Fig. 6d,e,r and Supplementary Fig. 7c–c″), whereas trabecular complexity and trabecular area were 30% and >300% above normal (Supplementary Fig. 6a), indicating defective compaction. Cardiomyocyte proliferation was 38% impaired in compact myocardium of E13.5 transgenic embryos (Fig. 6f,g,s). Unlike the thick compact myocardium with some compacting trabeculae in WT neonate mice (Fig. 6h–h″), $MFng^{tg}$;*Tie2-Cre* neonates had thin compact myocardium and non-compacted trabeculae in both ventricles, with no effect on cardiomyocyte size (Fig. 6i–i″). N1ICD expression was impaired in the ventricles of E16.5 $MFng^{tg}$;*Tie2-Cre* mice (Fig. 6j–k′,t), indicating that forced *MFng* endocardial expression disrupts Notch activation.

Hey2 expression in E16.5 $MFng^{tg}$;*Tie2-Cre* mice delineated the thin compact myocardium and extended towards but did not reach the trabeculae tip (compare Fig. 6l,m), whereas *Bmp10* and *Cx40* were restricted to the distal trabeculae tip (compare Fig. 6n–q). Indeed, *Hey2* and *Bmp10* (or *Cx40*) expression in the trabeculae were complementary (compare Fig. 6m,o,q). In the $MFng^{tg}$;*Tie2-Cre* ventricle, compact myocardium cardiomyocytes ($Hey2^{+}$, Fig. 6m) seemed to enter the trabeculae and form an ‘intermediate myocardium’ ($Hey2^{+}$, $Bmp10^{-}$, $Cx40^{-}$, Fig. 6m) defining a boundary between compact and trabecular myocardium ($Hey2^{-}$, $Bmp10^{+}$, $Cx40^{+}$, Fig. 6o,q). A similar but more subtle phenotype was observed in $Jag2^{flox}$;*cTnT-Cre* and $Jag1^{flox}$;$Jag2^{flox}$;*cTnT-Cre* hearts (Fig. 4m,n,p,q,s,t) but not $Mib1^{flox}$;*cTnT-Cre* hearts[15].

Upregulated *MFng* expression in coronary endothelium (Fig. 6a) and loss of *Cx40* expression in coronaries of E16.5 $MFng^{tg}$;*Tie2-Cre* mice (Fig. 6q) suggests that ectopic MFng might also affect compaction through alteration of the development of coronaries.

Comparative gene profiling

RNA-seq of E15.5 WT, $Jag2^{flox}$;*cTnT-Cre*, $Jag1^{flox}$;$Jag2^{flox}$;*cTnT-Cre* and $MFng^{tg}$;*Tie2-Cre* hearts was performed and compared with those from $Jag1^{flox}$;*cTnT-Cre* (Fig. 3 and Supplementary Table 1) and $Mib1^{flox}$;*cTnT-Cre* mice[15]. $Jag2^{flox}$;*cTnT-Cre* hearts showed differential expression of 41 genes (31 upregulated, 10 downregulated), $Jag1^{flox}$;$Jag2^{flox}$;*cTnT-Cre* hearts showed 474 genes (320 upregulated, 154 downregulated) and $MFng^{tg}$;*Tie2-Cre* hearts showed 1,561 (979 upregulated, 582 downregulated; Fig. 7a and Supplementary Table 1). $Jag1^{flox}$;*cTnT-Cre* and $Jag2^{flox}$;*cTnT-Cre* mutants shared 7 differentially expressed genes, $Jag1^{flox}$;*cTnT-Cre* and $Jag1^{flox}$;$Jag2^{flox}$;*cTnT-Cre* mutants 73 genes and $Jag2^{flox}$;*cTnT-Cre* and $Jag1^{flox}$;$Jag2^{flox}$;*cTnT-Cre* mutants 20 (Fig. 7b). $Jag1^{flox}$;$Jag2^{flox}$;*cTnT-Cre* and $Mib1^{flox}$;*cTnT-Cre* mutants shared 51 genes, $Jag1^{flox}$;$Jag2^{flox}$;*cTnT-Cre* and $MFng^{tg}$;*Tie2-Cre* 160 and $MFng^{tg}$;*Tie2-Cre* and $Mib1^{flox}$;*cTnT-Cre* 127 (Fig. 7b).

The heat map in Fig. 7c shows the 319 genes differentially expressed in at least two of the five mutant genotypes. *Jag2* inactivation affected fewer genes (41) than *Jag1* (97), but many more genes were affected in the double $Jag1^{flox}$;$Jag2^{flox}$;*cTnT-Cre* mutant (474), indicating

a synergistic effect of simultaneous inactivation (Fig. 7c). *MFng^{tg};Tie2-Cre* mice presented the largest number of deregulated genes, and genes shared with *Jag1^{flox};Jag2^{flox};cTnT-Cre* mutants generally changed in the same direction (Fig. 7c). The profile of *Mib1^{flox};cTnT-Cre* mutants was different, with expression of several deregulated genes showing the opposite changes to *Jag1^{flox};Jag2^{flox};cTnT-Cre* or *MFng^{tg};Tie2-Cre* mice (Fig. 7c).

GO analysis (Fig. 7d and Supplementary Table 1) identified alterations in genes involved in angiogenesis and vascular development, including the endocardial/endothelial Notch target *Hey2* (refs 35,36) in at least two genotypes. *Hey2* expression was down-regulated in *Jag1^{flox};Jag2^{flox};cTnT-Cre* and *MFng^{tg};Tie2-Cre* mice and upregulated in *Mib1^{flox};cTnT-Cre* mice (Fig. 7d and Supplementary Table 1 and ref. 15), reflecting its expanded expression from the compact myocardium to the large, non-compacted trabeculae[15]. Some of the deregulated genes in this category are involved in coronary artery development (*Cxcl12*; ref. 26, *Hey2*; ref. 37) and their down-regulated expression suggested defective coronary development in *Jag1^{flox};Jag2^{flox};cTnT-Cre* or *MFng^{tg};Tie2-Cre* mice. Genes involved in cardiac fibrosis (*Ctgf* (ref. 38), *Tgfβ1* (ref. 39)) were upregulated in *Jag1^{flox};Jag2^{flox};cTnT-Cre* and *MFng^{tg};Tie2-Cre* mice. A second GO category included cell-cycle and proliferation genes, in which negative cell-cycle regulators (*Cdkn1a/p21*, *Plk2*, *Rps6ka2* and *Romo1*) were upregulated in all genotypes except *Mib1^{flox};cTnT-Cre* mice (Fig. 7d). These results fit with the reduced cardiomyocyte proliferation in *Jag1* and *Jag2* mutants (Figs 3n and 4l) but not *Mib1^{flox};cTnT-Cre* mice[15] (Supplementary Fig. 6b–d′). Cell-death-related genes were deregulated in *Jag2^{flox};cTnT-Cre*, *Jag1^{flox};Jag2^{flox};cTnT-Cre* and *MFng^{tg};Tie2-Cre* hearts, including the apoptosis inhibitors *Spp1*, *Bcl6*, *Prnd* and *Bcl2l11* (downregulated) and the pro-apoptotic gene *Cish* (upregulated), suggesting altered cardiac cell homeostasis. Similar to what was found in *Dll4^{flox}* and *Notch1^{flox}* mutants (Fig. 1l), Semaphorin and Ephrin–Eph family members involved in cellular motion, axonal guidance and migration were deregulated. Semaphorins play key functions in cardiac morphogenesis and vascular patterning[40,41]. One down-regulated gene, *Efnb3*, is associated with the cardiac hypertrophic response in adult heart[42]. Genes related to dilated, hypertrophic and arrhythmogenic right ventricular cardiomyopathy (DCM, HCM and ARVC) were deregulated in *Jag1^{flox};cTnT-Cre*, *Jag1^{flox};Jag2^{flox};cTnT-Cre*, *MFng^{tg};Tie2-Cre* and *Mib1^{flox};cTnT-Cre* mice. Genes required for heart morphogenesis (*Nkx2.5*, *Adamts1*, *Smad7*, *Gaa* and *Eng*) were upregulated in *Jag1^{flox};Jag2^{flox};cTnT-Cre* mutants, whereas *Bmp10* and *ErbB4* expression changed in opposite directions in *MFng^{tg};Tie2-Cre* and *Mib1^{flox};cTnT-Cre* mice. Last, a set of genes encoding voltage-dependent potassium and calcium channels (*Kcnd3*, *Kcne1*, *Kcne3*, *Kcnd2* and *Cacna1g*) was deregulated in *Jag1^{flox};cTnT-Cre*, *MFng^{tg};Tie2-Cre* and *Mib1^{flox};cTnT-Cre* mice.

DISCUSSION

Our studies demonstrate that heart chamber development is coordinated through sequential Notch1 receptor activation in the endocardium, first by endocardially expressed Dll4 and later by Jag1 and Jag2 signalling from the myocardium. This temporally patterned Notch1 activation is determined by MFng and elicits different morphogenetic processes in the developing ventricles: the early, MFng-favoured endocardial Dll4–Notch1 signalling promotes cardiomyocyte proliferation and differentiation leading to trabeculation. The late,

myocardial Jag1/Jag2–endocardial Notch1 signalling, occurring after MFng (and Dll4) downregulation in the endocardium, supports myocardial patterning, maturation and compaction. Simultaneously, coronary endothelial Dll4 signalling to the Fng-modified-Notch1 receptor stimulates coronary vessel development.

RNA-seq of endocardial-specific *Dll4* or *Notch1* mutant hearts shows deregulation of a set of genes involved in crucial cellular processes, signalling, cardiovascular development and disease. *Gpr126* is of particular interest because its expression is dependent on Notch signalling in endothelial cells, zebrafish and mouse. Moreover, targeted *Gpr126* inactivation in mice disrupts trabeculation, revealing its crucial function in chamber development[22]. Work in zebrafish showed that an amino-terminal Gpr126 fragment rescues the trabeculation phenotype of *gpr126* morphants[22], suggesting that this fragment can function as a paracrine signal instructing adjacent trabecular cardiomyocytes. In response to Notch, Gpr126 might influence the proliferation and differentiation of neighbouring cardiomyocytes within the developing chamber. Accordingly, cardiomyocyte proliferation, essential for ventricular growth, is affected in endocardial *Dll4* and *Notch1* mutants. Indeed, we reported defective cardiomyocyte proliferation in *RBPJk/CBF1* mutants, accompanied by reduced *Bmp10* expression[12]. RNA-seq revealed increased expression of various negative cell-cycle regulators, suggesting that Notch signalling plays a general role in regulating cardiomyocyte proliferation. Proliferation and differentiation of embryonic cardiomyocytes are intimately connected[43] and our data suggest that Notch regulates both processes. Gene profiling revealed no significant changes in *EfnB2* or *Nrg1*, despite their downregulation after endothelial *Dll4* deletion in the ISH analysis and their roles downstream of Notch during trabeculation[12]. This discrepancy might reflect the low expression of *EfnB2* and *Nrg1* in WT heart and the strict criteria for considering a gene-expression change as significant.

Jag1 is non-essential for trabeculation but is required for ventricular maturation. *Jag1* inactivation in embryonic myocardium generated mice with a dilated heart, a thin compact myocardium, reduced ejection fraction and cardiomyopathy with systolic dysfunction. Myocardium-specific *Jag1* mutants showed impaired proliferation and elevated p21 expression in compact myocardium cardiomyocytes, findings supported by the RNA-seq. Expression of various chamber-patterning markers was also impaired, indicating that Jag1 is required for ventricular patterning and maturation. Myocardial Jag1 mutants, like endocardial *Dll4* mutants, showed reduced *Gpr126* expression, indicating Gpr126 as an important Notch effector throughout chamber development. Myocardial expression of *Jag2* increases from E12.5, mirroring *Jag1* expression. *Jag2* deletion also disrupts chamber maturation, and combined *Jag1* and *Jag2* deletion triggers a severe chamber phenotype reminiscent of LVNC.

MFng is a crucial temporal modulator of Notch ligand–receptor interaction during ventricular development. *In vitro* experiments show that in the absence of MFng, Dll4, Jag1 and Jag2 activate Notch to similar levels and that pairwise combinations of these ligands have an additive effect. In the presence of MFng, Dll4 becomes a Notch1 superactivator, but Jag1 and Jag2 activate Notch1 quite poorly, and do not affect the response to Dll4. The function of MFng as a Notch modulator has been described in embryonic vasculature, where Jag1 is co-expressed with Dll4 in endothelial cells and inhibits Notch activation[31]. In the

developing ventricle the situation is different because Dll4 and Jag1 are expressed in different cell types. This MFng–Dll4–Notch1 relationship also exists in the coronaries, as indicated by our loss-of-function data showing that MFng and Dll4 are required for coronary vessel development and thus indirectly for compaction. Ectopic *MFng* overexpression in vascular endothelium and endocardium of *MFng^{tg};Tie2-Cre* mice causes a severe, LVNC-like chamber phenotype. RNA-seq identified a large set of differentially expressed genes overlapping those affected in *Jag1^{flox};Jag2^{flox};cTnT-Cre* mice. Thus, the data indicate that *MFng* overexpression throughout the endocardium effectively blocks Jag1 and Jag2 myocardial signalling to Notch1.

The chamber-patterning defects in *Jag2^{flox};cTnT-Cre*, *Jag1^{flox};Jag2^{flox};cTnT-Cre* and *MFng^{tg};Tie2-Cre* mice are emphasized by the detection of an 'intermediate myocardium' (*Hey2^{+}*) in the trabeculae, proximal to the thin compact myocardium (*Hey2^{+}*), in addition to the distal trabecular myocardium (*Hey2^{-}*,*Bmp10^{+}*, *Cx40^{+}*). Supplementary Fig. 7 illustrates a feature common to all Notch mutants affecting compaction analysed here or previously[15]: the structural chamber defects are more severe in the right ventricle, perhaps reflecting the different developmental origins of the ventricular chambers[44].

Our results are summarized in Fig. 8. Inactivation of the ubiquitin ligase MIB1 causes LVNC in mice and humans[15]. The current findings show that combined myocardial inactivation of *Jag1* and *Jag2* also causes LVNC, suggesting that both ligands are Mib1 substrates in the myocardium. This is supported by the LVNC-like phenotype after forced endocardial *MFng* expression (Fig. 8). Our findings shed light on the molecular mechanisms orchestrating ventricular chamber development, and the coordination between compaction and the formation of the coronary vessels that nourish the mature ventricles. Understanding these developmental processes has important implications for the management of heart disease.

METHODS

Mouse strains and genotyping

Animal studies were approved by the CNIC Animal Experimentation Ethics Committee and by the Community of Madrid (Ref. PROEX 118/15). All animal procedures conformed to EU Directive 2010/63EU and Recommendation 2007/526/EC regarding the protection of animals used for experimental and other scientific purposes, enforced in Spanish law under Real Decreto 1201/2005. Mouse strains were *CBF:H2B-Venus* (ref. 16), *Notch1* (ref. 45), *RBPJk* (ref. 46), *Tie2-Cre* (ref. 18), *Nfatc1-Cre* (ref. 4), *cTnT-Cre* (ref. 24), *Cdh5(PAC)-Cre^{ERT2}* (ref. 19), *Dll4^{flox}* (ref. 17), *Jag1^{flox}* (ref. 47), *Jag2^{flox}* (ref. 48), *Notch1^{flox}* (ref. 49), *Mib1^{flox}* (ref. 50). Fringe mutant strains were bred and maintained as described previously[34]. For the generation of *Rosa26-MFng* Tg mice (Acc. No. CDB0917K: http://www.cdb.riken.jp/arg/mutant%20mice%20list.html), a cDNA encoding a native form of murine *MFng* was cloned into a modified version of the *pROSA26-1* vector, preceded by the ubiquitous CAG promoter and a loxP-flanked 'Neo^{R}-STOP' cassette and followed by a frt-flanked IRES–EGFP cassette and a bovine polyadenylation sequence. Gene targeting was done with TT2 embryonic stem cells and confirmed by Southern blotting. Mice were

generated by injection of targeted embryonic stem cells into ICR embryos, and were backcrossed with the C57BL/6 strain. Details of genotyping will be provided on request.

Zebrafish experiments

Zebrafish were maintained and raised under standard conditions at 28 °C. We used WT AB and *mib*^{ta52b} fish[51]. WT embryos were treated for 15 h with RO4929097 (S1575, selleckchem.com, 10 μM) or with dimethylsulphoxide[23] (DMSO). All embryos were fixed at 48 hpf in 4% PFA overnight and processed for *in situ* hybridization (ISH) as described previously[52].

4-hydroxy-tamoxifen (4-OHT) induction

Dll4$^{flox/+}$*;Cdh5-Cre*$^{ERT/+}$ male mice were crossed with *Dll4*$^{flox/flox}$ females and pregnant females were administered with 4-OHT (H6278 Sigma) once by oral gavage at 12.5 days of gestation. Embryos were dissected at E15.5.

Histology and *in situ* hybridization

Haematoxylin–eosin (H&E) staining, *in situ* hybridization (ISH) on sections, and whole-mount ISH were performed as described previously[52,53]. Details of probes will be provided on request.

Whole-mount immunofluorescence

E9.5 *CBF:H2B-Venus* embryos were dissected and fixed for 2 h in 4% PFA at 4 °C. Embryos were permeabilized for 1 h with 0.5% Triton X-100/PBS and subsequently blocked for 1 h in Histoblock solution (5% goat serum, 3% BSA, 0.3% Tween-20 in PBS). Primary and secondary antibodies used are listed in Supplementary Table 2. After several washes in PBS-T (PBS containing 0.1% Tween-20) embryos were mounted in a 60 mm Petri dish with 1% agar. To detect endogenous GFP, fixed E9.5 *CBF:H2B-Venus; CBF:H2B-Venus;N1KO* and *CBF:H2B-Venus;RBPJkKO* embryos were imaged with a Zeiss 780 confocal microscope fitted with a ×20 objective with a dipping lens. *Z*-stacks were taken every 5 μm. 3D images were reconstructed with IMARIS software (Bitplane Scienific Software).

Immunohistochemistry

Paraffin sections (7 μm) were incubated overnight with primary antibodies, followed by 1 h incubation with a fluorescent-dye-conjugated secondary antibody. N1ICD, Dll4, Jag1 and p21 staining was performed using tyramide signal amplification[54,55] (TSA). All antibodies used are listed in Supplementary Table 2.

Quantification of incorporated BrdU, p21 and N1ICD

Cell proliferation was analysed by detection of BrdU incorporation[55]. For p21 and N1ICD quantification, positive nuclei were divided by the total number of nuclei counted on sections (≥4) in six embryos of each genotype. Images were processed with ImageJ software. Statistical significance was assessed by Student's *t*-test.

Quantification of compact myocardium thickness and trabecular complexity

The method used was a modification of that described in refs 56,57. Briefly, 7 μm paraffin sections from E9.5 WT and mutant hearts were stained with anti-CD31 and anti-MF20 to facilitate visualization of ventricular structures. In E16.5 WT and mutant hearts endocardial cells were stained with anti-endomucin and myocardium with anti-cTnT. Confocal images were obtained with a NIKON A1R confocal microscope. ImageJ software was used for the measurements. In E16.5 heart sections, left and right ventricles were analysed separately. For each measurement, settings were kept constant for all images using the scale bar recorded in each image as the reference distance. The thickness of the compact myocardium was measured by dividing the ventricle into two main regions: the apex (at the bottom of a transverse section) and the basal region (at the top; see Supplementary Fig. 7a). Several measurements were taken in each region and the mean was expressed in micrometres. The complexity of trabecular myocardium indicates the size of the trabecular mesh of myocardial fibres and is considered a landmark of cardiomyopathy[25]. It was represented as the mean ratio, expressed in micrometres, obtained by dividing the length of each trabecula by its thickness. The ratio of trabecular area and compact myocardial thickness was measured by dividing the surface occupied by trabeculae in the ventricle (μm^2) by the length of compact myocardium expressed in micrometres.

Imaging, photography and 3D reconstruction

E9.5 whole-embryos or hearts were imaged with a Zeiss 780 confocal microscope fitted with a ×20 objective with a dipping lens. *Z*-stacks were taken every 5 μm. 3D images were reconstructed with IMARIS software (Bitplane Scientific Software). WT E9.5 embryos were sectioned at 10 μm and stained for Dll4, Jag1 and N1ICD. Images were acquired with a confocal microscope (Leica TCS SPE) taking 10 optical sections per histological section. After acquisition, 3D reconstructions were performed as described previously[58] and the resulting surfaces were exported to Adobe Acrobat Professional 9 Extended version to generate 3D interactive pdf files[59].

Lentiviral production and infection

Full-length murine *Manic Fringe (MFng)* (ref. 31) was subcloned into the lentiviral vector pRLL-IRES-eGFP (Addgene). Concentrated lentiviruses expressing pRLL-IRES-eGFP or pRLL-MFng-IRES-eGFP were obtained as described previously[60]. Viruses were titrated in Jurkat cells, and infection efficiency (GFP-expressing cells) and cell death (propidium iodide staining) were monitored by flow cytometry.

Isolation and immortalization of MEVEC

Mouse embryonic ventricular endocardial cells (MEVEC) were obtained from ventricles of E10.5 embryos. Embryos were dissected in PBS and hearts were collected. Atria and the atrioventricular canal were removed and the remaining ventricles were mechanically dissociated. Isolated cells were collected in DMEM containing 20% FBS and centrifuged at 400*g* for 5 min. The cells were finally resuspended in 500 μl culture medium (DMEM, 20% FBS supplemented with penicillin/streptomycin and 100 μg ml^{-1} endothelial cell growth supplement (ECGS) (Sigma-Aldrich)), and seeded into one well of a MW24 plate pre-

treated with collagen type I (4.08 mg ml^{-1}; BD Bioscience). After 1 week, a confluent cobblestone morphology culture was observed and cells were transferred to one gelatinized p60 flask. MEVEC in passage 1 were infected with lentivirus expressing SV40-large T antigen in the presence of Polybrene (8 μg ml^{-1}). Overexpression of SV40-large T antigen was determined by qRT–PCR. MEVEC cultures expressed the chamber endocardial markers *Notch1*, *Dll4*, *Nfatc1, Nrg1* and *Gpr126* (Supplementary Fig. 8c) and maintained their endocardial phenotype and cobblestone morphology over 20–25 passages.

Cell culture

Human umbilical vein endothelial cells (HUVEC) were purchased from Lonza, and cultured on gelatin-coated dishes until passage 9 in EGM-2 complete medium (Lonza) supplemented with penicillin/streptomycin. For expression analysis by qPCR, HUVEC were pre-treated with 10 μM γ-secretase inhibitor (RO4929097, Selleckchem) or vehicle (DMSO) and stimulated with Notch ligands as described above for MEVEC. Bovine aortic endothelial cells (BAEC) were purchased from Lonza and cultured in DMEM supplemented with penicillin/streptomycin plus 10%FBS.

Luciferase assays with *Gpr126* genomic DNA fragments

The Evolutionary Conserved Region web platform (ECR; http://ecrbrowser.dcode.org) was used to identify RBPJ motifs in the *Gpr126* gene. Two conserved RBPJ-binding sites were found in the intronic region, flanking the fifth and sixth exon of human, monkey, rat and mouse *Gpr126*. In human the conserved RBPJ sites are separated by 445 base pairs (bp). Genomic DNA from HUVEC was used as a template to amplify 726 bp of *GPR126* containing the two conserved sites and the product was cloned into the KpnI and XhoI sites of the pGL3 promoter luciferase plasmid (Promega). The primer sequences were: 5′-ATGCGGTACCATTTATACTTGTTACTGTGC-3′ (forward, KpnI site underlined) and 5′-ATCGCTCGAGGGCCAAGAATTATAAAGAATGAG-3′ (reverse, XhoI site underlined). For luciferase assays we transiently co-transfected BAEC with the hGPR126 reporter plasmid (pGL3-hGPR126-Luciferase), Renilla plasmid, and increasing amounts of vector expressing the intracellular domain of Notch1 (0–200 ng) (pCS2-N1ICD). Twenty-four hours after transfection the cells were lysed, and luciferase activity was measured with the Dual Luciferase Assay System (Promega).

Notch stimulation with recombinant ligands and luciferase assays

For Notch stimulation with recombinant ligands, MW24 plates were incubated with anti-human-IgG-Fc, anti-mouse-IgG2a-Fc (Jackson), anti-His (Zymed), or a 1:1 mixture of antibodies (6.48 mg ml^{-1}) for 30 min at 37 °C. After washing with PBS, plates were blocked for 1 h at 37 °C with 10% FBS in DMEM. Recombinant Dll4 (mouse Dll4–His R&D Systems no. 1389-D4), Jagged1 (rat Jag1-Fc, R&D Systems no. 599–JG) or Jagged2 (mouse Jag2-Fc, R&D Systems no. 4748–JG) was diluted in PBS and added to the dishes individually or in a 1:1 mixture at a final concentration of 18 nM. After 2 h at 37 °C, wells were washed and *GFP*-MEVEC and *MFng*-MEVEC were incubated on the coated plates at subconfluency overnight. For luciferase assays, stimulated cells were transiently co-transfected with the Notch reporter plasmid pGL3-10xCBF1-Luciferase and pGL3-Renilla luciferase at a 5:1 ratio using Lipofectamine and Plus reagents (Life Technologies). Twenty

hours after transfection, luciferase activity was measured with the Dual Luciferase Assay System (Promega). Data are expressed as Firefly/*Renilla* luciferase ratios. Experiments were performed at least three times, with quadruplicate samples for each experiment. Data are presented as mean ± s.d. Differences were considered statistically significant at $P < 0.05$ (Student's *t*-test).

Quantitative RT–PCR

WT and mutant embryos at different stages were dissected in ice-cold PBS. Whole E8.5 hearts and ventricles of E9.5–14.5 embryos were separated from the rest of the body and RNA was extracted. For RNA extraction from cells stimulated *in vitro* with recombinant Notch ligands, the stimulation protocol was conducted as above in MW6 dishes and RNA was extracted after overnight incubation. Total RNA was purified using Trizol (Invitrogen). cDNA was synthesized with SuperScript III First Strand (Invitrogen), with 1 μg total RNA per reaction. Quantitative PCR was performed with Power SYBR Green Master Mix (Applied Biosystems, 4367659). Oligonucleotide sequences for real-time PCR analysis performed in this study are listed in Supplementary Table 3. Data are presented as mean ± s.d. Differences were considered statistically significant at $P < 0.05$ (Student's *t*-test).

RNA-Seq

RNA was isolated at E9.5 from whole hearts of WT and *Dll4^{flox};Nfatc1-Cre* embryos (32 per genotype), WT and *Notch1^{flox};Nfatc1-Cre* embryos (24 per genotype), and WT and *Dll4^{flox};Tie2-Cre* embryos (27 per genotype). RNA was pooled into four replicates for the first genotype pairs and three replicates for the last two genotype pairs. For *Jag1^{flox};cTnT-Cre* hearts, RNA was isolated from the ventricles of 12 WT and 12 mutant hearts at E15.5 and then pooled into three replicates. RNA was prepared using the standard Illumina TrueSeq RNA-Seq library preparation kit. Libraries were sequenced in a GAIIx Illumina sequencer using a 75 bp single end elongation protocol. For *Jag2^{flox};cTnT-Cre* and *Jag1^{flox};Jag2^{flox};cTnT-Cre* hearts, RNA was isolated from the ventricles of 8 WT and 12 mutant hearts at E15.5 and then pooled into two and three replicates respectively. For *MFng^{GOF};Tie2-Cre* hearts, RNA was isolated from the ventricles of 16 WT and 16 GOF hearts at E15.5 and then pooled into four replicates each. RNA was prepared using the NEBNext Ultra RNA Library Prep Kit for Illumina. Libraries were sequenced in a HiSeq2500 Illumina sequencer using a 61 bp single end elongation protocol. Sequenced reads were QC and pre-processed using cutadapt v1.6 (ref. 61) to remove adaptor contaminants. Resulting reads were aligned and gene expression quantified using RSEM v1.2.3 (ref. 62) over mouse reference GRCm38 and Ensembl genebuild 70. Gene differential expression was analysed using the EdgeR R package[63]. Data from *Dll4^{flox};Tie2-Cre* and *Dll4^{flox};Nfatc1-Cre* experiments were analysed together, as were data from *Dll4^{flox};Nfatc1-Cre* and *Notch1^{flox};Nfatc1-Cre* experiments, by applying batch correction using ComBat (ref. 64) to account for experimental differences. For *Jag1^{flox}* and *Jag2^{flox}* single and double Jag1^{flox};Jag2^{flox};*cTnT-Cre* experiments, data were analysed together applying batch correction to account for technical differences and adding the genotypes of both alleles as covariates. *Mib^{flox};cTnT-Cre* (E14.5) RNA-Seq from ref. 15 was reanalysed using the GRCm38 genebuild 70 reference. Genes showing altered expression with adjusted $P < 0.05$ were considered differentially expressed. For the set of differentially expressed genes a

functional analysis was performed using Ingenuity Pathway Analysis Software and DAVID (ref. 65), and some of the enriched processes were selected according to relevant criteria related to the biological process studied. Unsupervised hierarchical clustering with Genesis Software[66] was used to group genes according to the similarity of their expression profiles across the different Dll4 and Notch1 deficiency experiments. Using a new R visualization package called GOPlot, a chord plot[67,68] was generated to better visualize the relationships between genes and the selected enriched processes.

Accession number

Data are deposited in the NCBI GEO database under accession number GSE67889.

Ultrasound

Left ventricle (LV) function and wall thickness were analysed by transthoracic echocardiography in male mice at 6 and 9 months of age. Mice were mildly anaesthetized by inhalation of isoflurane/oxygen (1–2%/98.75%) adjusted to obtain a target heart rate of 450 ± 50 beats per minute and examined with a 30 MHz transthoracic echocardiography probe. Images were obtained with Vevo 2100 (VisualSonics) from *Jag1^{flox};cTnT-Cre*, *Jag2^{flox};cTnT-Cre* and WT littermates. LV long-axis M-Mode views were obtained as described previously[69]. From these images, interventricular septum end-diastolic thickness was measured, and LV systolic function was assessed by estimating LV shortening fraction and LV ejection fraction[69].

Cardiac MRI

Six-month-old male mice were anaesthetized by inhalation of isoflurane/oxygen (2%) and monitored by ECG and breathing rhythm (Model 1025, S.A. Instruments). Images were acquired with an Agilent/Varian 7 T system equipped with a DD1 console and an active shielded 205/120 gradient insert coil with 130 mT m^{-1} maximum strength and a combination of volume (transmission, TX) and two-channel phased array (reception, RX) coils (Rapid Biomedical GmbH) for transmit/receipt. Data were collected in a triggered cine gradient echo sequence with TE = 1.45 ms and TR 7 ms, FA 25°, 20 cardiac phases, and NA (number of averages) = 3. A total of 13 contiguous slices in the short-axis view were acquired, with a slice thickness of 0.8 mm. The field of view was 3 × 3 cm, with a 256 × 256 matrix.

Left ventricle (LV) and right ventricle (RV) function, end-diastolic volume, mass and wall thickness of the right ventricle were estimated by the Simpson method, which sums the RV end-diastolic areas from the 13 slices in the short-axis view and multiplies this figure by the 0.8 mm slice thickness. Images were processed using OsiriX (Pixmeo) and Medis MASS software (The Netherlands) to calculate every RV area by segmentation of end-diastolic epicardial and endocardial edge[70].

Statistical analysis

Statistical analysis was carried out using Prism 5 (GraphPad). All statistical tests were performed using two-sided, unpaired Student's *t*-tests except for Fig. 2j where numerical data are presented as mean ± s.e.m; *$P < 0.05$, **$P < 0.01$ and ***$P < 0.001$. Sample size

was chosen empirically according to previous experience in the calculation of experimental variability. No statistical method was used to predetermine sample size. All experiments were carried out with at least three biological replicates. The numbers of animals used are described in the corresponding figure legends. For adult image analysis by echo and CMRI we ensured that experimental groups were balanced in terms of animal age, sex and weight unless otherwise specified. Animals were genotyped before the experiment and were caged together and treated in the same way. Variance was comparable between groups throughout the manuscript. We chose the appropriate tests according to the data distributions. The experiments were not randomized. The investigators were not blinded to allocation during experiments and outcome assessment except for adult image analysis. Panels in Figs 1a–h′,m–n′,p–q′; 2a–f′,k–p′; 3d–m′; 4a,b–b′,f–k′,m–s; 5a,e–j′,i–m; 6a,c,d–i′,j–o and Supplementary Figs 1a–h; 2a,c,d–f′; 3a–p′; 5a,5c–f′; 6c–d′; 7a–d″ and 8a show a representative image of at least three independent experiments.

Supplementary Material

Refer to Web version on PubMed Central for supplementary material.

ACKNOWLEDGEMENTS

We thank Y. Fukushima (Osaka U., Japan) for help with the generation of the *R26-MFng* targeting vector, RIKEN CDB (Japan) for producing the chimaeric mice, the CNIC Genomics Unit for RNA-seq, the CNIC Advance Imaging Unit for CMRI analysis, B. Zhou (Albert Einstein College, NYC, USA) for the *NFATc1-Cre* driver line, A. Martín-Pendas (CSIC, Salamanca, Spain), P. Muñoz-Canoves (UPF, Barcelona, Spain) and J. M. Pérez-Pomares (Málaga U., Spain) for critical reading of the manuscript and S. Bartlett (CNIC) and K. McCreath for English editing. Funds were from grants SAF2013-45543-R, RD12/0042/0005 (RIC) and RD12/0019/0003 (TERCEL) from the Spanish Ministry of Economy and Competitiveness (MINECO), FP7-ITN 215761 (NotchIT) and 28600 (CardioNeT) from the EU and a grant from the BBVA Foundation for Research in Biomedicine (2014), all to J.L.d.l.P. G.D'A. holds a PhD fellowship linked to grant FP7-ITN 215761 (NotchIT). The MINECO and the Pro-CNIC Foundation support the CNIC.

References

1. Sedmera D, Pexieder T, Vuillemin M, Thompson RP, Anderson RH. Developmental patterning of the myocardium. Anat. Rec. 2000; 258:319–337. [PubMed: 10737851]
2. Moorman AF, Christoffels VM. Cardiac chamber formation: development, genes, and evolution. Physiol. Rev. 2003; 83:1223–1267. [PubMed: 14506305]
3. Tevosian SG, et al. FOG-2, a cofactor for GATA transcription factors, is essential for heart morphogenesis and development of coronary vessels from epicardium. Cell. 2000; 101:729–739. [PubMed: 10892744]
4. Wu B, et al. Endocardial cells form the coronary arteries by angiogenesis through myocardial-endocardial VEGF signaling. Cell. 2012; 151:1083–1096. [PubMed: 23178125]
5. Wessels A, Sedmera D. Developmental anatomy of the heart: a tale of mice and man. Physiol. Genomics. 2003; 15:165–176. [PubMed: 14612588]
6. Ritter M, et al. Isolated noncompaction of the myocardium in adults. Mayo Clin. Proc. 1997; 72:26–31. [PubMed: 9005281]
7. Towbin JA. Left ventricular noncompaction: a new form of heart failure. Heart Fail. Clin. 2010; 6:453–469. [PubMed: 20869646]
8. Maron BJ, et al. Contemporary definitions and classification of the cardiomyopathies: an American Heart Association Scientific Statement from the Council on Clinical Cardiology, Heart Failure and Transplantation Committee; Quality of Care and Outcomes Research and Functional Genomics and Translational Biology Interdisciplinary Working Groups; and Council on Epidemiology and Prevention. Circulation. 2006; 113:1807–1816. [PubMed: 16567565]

9. Captur G, Nihoyannopoulos P. Left ventricular non-compaction: genetic heterogeneity, diagnosis and clinical course. Int. J. Cardiol. 2010; 140:145–153. [PubMed: 19664830]
10. Sarma RJ, Chana A, Elkayam U. Left ventricular noncompaction. Prog. Cardiovasc. Dis. 2010; 52:264–273. [PubMed: 20109597]
11. Arbustini E, Weidemann F, Hall JL. Left ventricular noncompaction: a distinct cardiomyopathy or a trait shared by different cardiac diseases? J. Am. Coll. Cardiol. 2014; 64:1840–1850. [PubMed: 25443708]
12. Grego-Bessa J, et al. Notch signaling is essential for ventricular chamber development. Dev. Cell. 2007; 12:415–429. [PubMed: 17336907]
13. Itoh M, et al. Mind bomb is a ubiquitin ligase that is essential for efficient activation of Notch signaling by Delta. Dev. Cell. 2003; 4:67–82. [PubMed: 12530964]
14. Kopan R, Ilagan MX. The canonical Notch signaling pathway: unfolding the activation mechanism. Cell. 2009; 137:216–233. [PubMed: 19379690]
15. Luxan G, et al. Mutations in the NOTCH pathway regulator MIB1 cause left ventricular noncompaction cardiomyopathy. Nat. Med. 2013; 19:193–201. [PubMed: 23314057]
16. Nowotschin S, Xenopoulos P, Schrode N, Hadjantonakis AK. A bright single-cell resolution live imaging reporter of Notch signaling in the mouse. BMC Dev. Biol. 2013; 13 http://dx.doi.org/10.1186/1471-213X-13-15.
17. Koch U, et al. Delta-like 4 is the essential, nonredundant ligand for Notch1 during thymic T cell lineage commitment. J. Exp. Med. 2008; 205:2515–2523. [PubMed: 18824585]
18. Kisanuki YY, et al. Tie2-Cre transgenic mice: a new model for endothelial cell-lineage analysis in vivo. Dev. Biol. 2001; 230:230–242. [PubMed: 11161575]
19. Wang Y, et al. Ephrin-B2 controls VEGF-induced angiogenesis and lymphangiogenesis. Nature. 2010; 465:483–486. [PubMed: 20445537]
20. Bjarnadottir TK, Fredriksson R, Schioth HB. The adhesion GPCRs: a unique family of G protein-coupled receptors with important roles in both central and peripheral tissues. Cell Mol. Life Sci. 2007; 64:2104–2119. [PubMed: 17502995]
21. Waller-Evans H, et al. The orphan adhesion-GPCR GPR126 is required for embryonic development in the mouse. PLoS ONE. 2010; 5:e14047. [PubMed: 21124978]
22. Patra C, et al. Organ-specific function of adhesion G protein-coupled receptor GPR126 is domain-dependent. Proc. Natl Acad. Sci. USA. 2013; 110:16898–16903. [PubMed: 24082093]
23. Munch J, Gonzalez-Rajal A, de la Pompa JL. Notch regulates blastema proliferation and prevents differentiation during adult zebrafish fin regeneration. Development. 2013; 140:1402–1411. [PubMed: 23344707]
24. Jiao K, et al. An essential role of Bmp4 in the atrioventricular septation of the mouse heart. Genes Dev. 2003; 17:2362–2367. [PubMed: 12975322]
25. Captur G, et al. Abnormal cardiac formation in hypertrophic cardiomyopathy: fractal analysis of trabeculae and preclinical gene expression. Circ. Cardiovasc. Genet. 2014; 7:241–248. [PubMed: 24704860]
26. Ivins S, et al. The CXCL12/CXCR4 axis plays a critical role in coronary artery development. Dev. Cell. 2015; 33:455–468. [PubMed: 26017770]
27. Cavallero S, et al. CXCL12 signaling is essential for maturation of the ventricular coronary endothelial plexus and establishment of functional coronary circulation. Dev. Cell. 2015; 33:469–477. [PubMed: 26017771]
28. Tian X, Pu WT, Zhou B. Cellular origin and developmental program of coronary angiogenesis. Circ. Res. 2015; 116:515–530. [PubMed: 25634974]
29. Panin VM, Papayannopoulos V, Wilson R, Irvine KD. Fringe modulates Notch-ligand interactions. Nature. 1997; 387:908–912. [PubMed: 9202123]
30. Yang LT, et al. Fringe glycosyltransferases differentially modulate Notch1 proteolysis induced by Delta1 and Jagged1. Mol. Biol. Cell. 2005; 16:927–942. [PubMed: 15574878]
31. Benedito R, et al. The notch ligands Dll4 and Jagged1 have opposing effects on angiogenesis. Cell. 2009; 137:1124–1135. [PubMed: 19524514]

32. McKenzie GJ, et al. Nuclear Ca^{2+} and CaM kinase IV specify hormonal- and Notch-responsiveness. J. Neurochem. 2005; 93:171–185. [PubMed: 15773917]
33. Timmerman LA, et al. Notch promotes epithelial-mesenchymal transition during cardiac development and oncogenic transformation. Genes Dev. 2004; 18:99–115. [PubMed: 14701881]
34. Moran JL, et al. Manic fringe is not required for embryonic development, and fringe family members do not exhibit redundant functions in the axial skeleton, limb, or hindbrain. Dev. Dynam. 2009; 238:1803–1812.
35. Luna-Zurita L, et al. Integration of a Notch-dependent mesenchymal gene program and Bmp2-driven cell invasiveness regulates murine cardiac valve formation. J. Clin. Invest. 2010; 120:3493–3507. [PubMed: 20890042]
36. Fischer A, Schumacher N, Maier M, Sendtner M, Gessler M. The Notch target genes Hey1 and Hey2 are required for embryonic vascular development. Genes Dev. 2004; 18:901–911. [PubMed: 15107403]
37. Watanabe T, Koibuchi N, Chin MT. Transcription factor CHF1/Hey2 regulates coronary vascular maturation. Mech. Dev. 2010; 127:418–427. [PubMed: 20619341]
38. Leask A. Getting to the heart of the matter: new insights into cardiac fibrosis. Circ. Res. 2015; 116:1269–1276. [PubMed: 25814687]
39. Hinz B. The extracellular matrix and transforming growth factor-β1: tale of a strained relationship. Matrix Biol. 2015; 47:54–65. [PubMed: 25960420]
40. Epstein JA, Aghajanian H, Singh MK. Semaphorin signaling in cardiovascular development. Cell Metab. 2015; 21:163–173. [PubMed: 25651171]
41. Toyofuku T, et al. Guidance of myocardial patterning in cardiac development by Sema6D reverse signalling. Nat. Cell Biol. 2004; 6:1204–1211. [PubMed: 15543137]
42. Dirkx E, et al. Nfat and miR-25 cooperate to reactivate the transcription factor Hand2 in heart failure. Nat. Cell Biol. 2013; 15:1282–1293. [PubMed: 24161931]
43. Hertig CM, Kubalak SW, Wang Y, Chien KR. Synergistic roles of neuregulin-1 and insulin-like growth factor-I in activation of the phosphatidylinositol 3-kinase pathway and cardiac chamber morphogenesis. J. Biol. Chem. 1999; 274:37362–37369. [PubMed: 10601306]
44. Kelly RG, Buckingham ME, Moorman AF. Heart fields and cardiac morphogenesis. Cold Spring Harb. Perspect. Med. 2014; 4:a015750. [PubMed: 25274757]
45. Conlon RA, Reaume AG, Rossant J. Notch1 is required for the coordinate segmentation of somites. Development. 1995; 121:1533–1545. [PubMed: 7789282]
46. Oka C, et al. Disruption of the mouse RBP-J kappa gene results in early embryonic death. Development. 1995; 121:3291–3301. [PubMed: 7588063]
47. Mancini SJ, et al. Jagged1-dependent Notch signaling is dispensable for hematopoietic stem cell self-renewal and differentiation. Blood. 2005; 105:2340–2342. [PubMed: 15550486]
48. Xu J, Krebs LT, Gridley T. Generation of mice with a conditional null allele of the Jagged2 gene. Genesis. 2010; 48:390–393. [PubMed: 20533406]
49. Radtke F, et al. Deficient T cell fate specification in mice with an induced inactivation of Notch1. Immunity. 1999; 10:547–558. [PubMed: 10367900]
50. Koo BK, et al. An obligatory role of mind bomb-1 in notch signaling of mammalian development. PLoS ONE. 2007; 2:e1221. [PubMed: 18043734]
51. Zhang C, Li Q, Lim CH, Qiu X, Jiang YJ. The characterization of zebrafish antimorphic mib alleles reveals that Mib and Mind bomb-2 (Mib2) function redundantly. Dev. Biol. 2007; 305:14–27. [PubMed: 17331493]
52. de la Pompa JL, et al. Conservation of the Notch signalling pathway in mammalian neurogenesis. Development. 1997; 124:1139–1148. [PubMed: 9102301]
53. Kanzler B, Kuschert SJ, Liu YH, Mallo M. Hoxa-2 restricts the chondrogenic domain and inhibits bone formation during development of the branchial area. Development. 1998; 125:2587–2597. [PubMed: 9636074]
54. Del Monte G, Grego-Bessa J, Gonzalez-Rajal A, Bolos V, de la Pompa JL. Monitoring Notch1 activity in development: evidence for a feedback regulatory loop. Dev. Dynam. 2007; 236:2594–2614.

55. Del Monte G, et al. Differential notch signaling in the epicardium is required for cardiac inflow development and coronary vessel morphogenesis. Circ. Res. 2011; 108:824–836. [PubMed: 21311046]
56. Yang J, et al. Inhibition of Notch2 by Numb/Numblike controls myocardial compaction in the heart. Cardiovasc. Res. 2012; 96:276–285. [PubMed: 22865640]
57. Chen H, et al. Analysis of ventricular hypertrabeculation and noncompaction using genetically engineered mouse models. Pediatr. Cardiol. 2009; 30:626–634. [PubMed: 19396388]
58. Soufan AT, et al. Regionalized sequence of myocardial cell growth and proliferation characterizes early chamber formation. Circ. Res. 2006; 99:545–552. [PubMed: 16888243]
59. de Boer BA, et al. The interactive presentation of 3D information obtained from reconstructed datasets and 3D placement of single histological sections with the 3D portable document format. Development. 2011; 138:159–167. [PubMed: 21138978]
60. Esteban V, et al. Regulator of calcineurin 1 mediates pathological vascular wall remodeling. J. Exp. Med. 2011; 208:2125–2139. [PubMed: 21930771]
61. Martin M. Cutadapt removes adapter sequences from high-throughput sequencing reads. EMB J. 2011; 17:10–12.
62. Li B, Dewey CN. RSEM: accurate transcript quantification from RNA-Seq data with or without a reference genome. BMC Bioinform. 2011; 12 http://dx.doi.org/10.1186/1471-2105-12-323.
63. Robinson MD, McCarthy DJ, Smyth GK. edgeR: a Bioconductor package for differential expression analysis of digital gene expression data. Bioinformatics. 2010; 26:139–140. [PubMed: 19910308]
64. Johnson WE, Li C, Rabinovic A. Adjusting batch effects in microarray expression data using empirical Bayes methods. Biostatistics. 2007; 8:118–127. [PubMed: 16632515]
65. Huang da W, Sherman BT, Lempicki RA. Systematic and integrative analysis of large gene lists using DAVID bioinformatics resources. Nat. Protoc. 2009; 4:44–57. [PubMed: 19131956]
66. Sturn A, Quackenbush J, Trajanoski Z. Genesis: cluster analysis of microarray data. Bioinformatics. 2002; 18:207–208. [PubMed: 11836235]
67. Walter W, Sanchez-Cabo F, Ricote M. GOplot: an R package for visually combining expression data with functional analysis. Bioinformatics. 2015; 31:2912–2914. [PubMed: 25964631]
68. Krzywinski M, et al. Circos: an information aesthetic for comparative genomics. Genome Res. 2009; 19:1639–1645. [PubMed: 19541911]
69. Cruz-Adalia A, et al. CD69 limits the severity of cardiomyopathy after autoimmune myocarditis. Circulation. 2010; 122:1396–1404. [PubMed: 20855659]
70. van de Weijer T, et al. Geometrical models for cardiac MRI in rodents: comparison of quantification of left ventricular volumes and function by various geometrical models with a full-volume MRI data set in rodents. Am. J. Physiol. Heart Circ. Physiol. 2012; 302:H709–H715. [PubMed: 22101529]

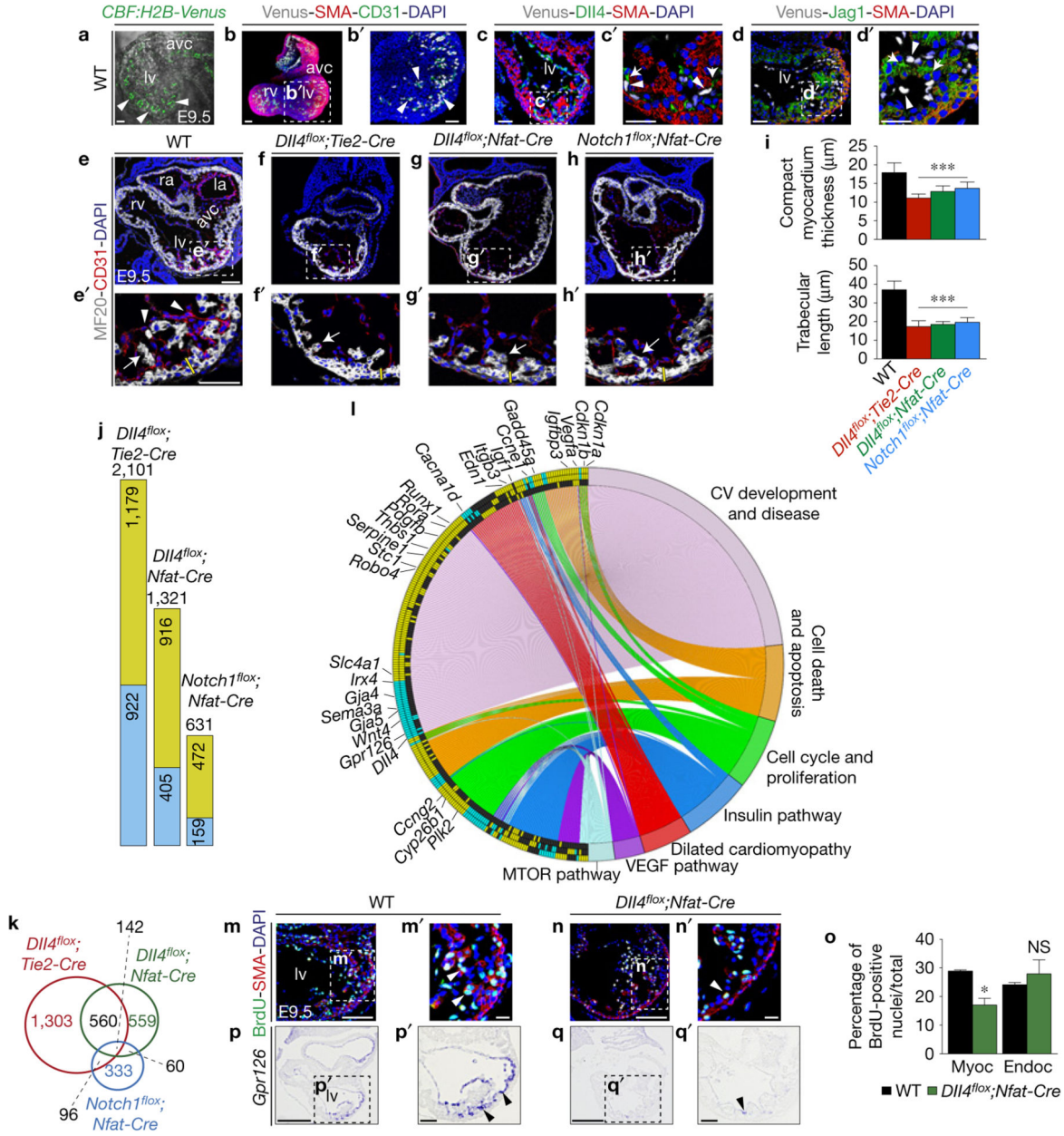

Figure 1.

Dll4–Notch1 signalling abrogation disrupts trabeculation and chamber-gene expression. (**a**) E9.5 WT *CBF:H2B-Venus* embryo, two-photon whole-mount image, left ventricle. Arrowheads indicate Venus expression. (**b,b′**) E9.5 WT *CBF:H2B-Venus* heart, whole-mount view of immunohistochemistry for Venus (grey), smooth-muscle actin (SMA, red) and CD31 (Pecam1) (green). (**c,c′**) E9.5 WT *CBF:H2B-Venus* heart, Dll4 (green), SMA (red) and GFP (grey) immunohistochemistry. (**d,d′**) E9.5 WT *CBF:H2B-Venus* heart, Jag1 (green), SMA (red) and GFP (grey) immunohistochemistry. Scale bars, 50 μm. (**e–h′**) Sarcomeric myosin (MF20) and CD31 immunohistochemistry in E9.5 WT (**e,e′**), *Dll4*$^{flox/flox}$*;Tie2-Cre/+*(*Dll4*^{flox}*;Tie2-Cre*) (**f,f′**), *Dll4*$^{flox/flox}$*;Nfatc1pan-Cre/+* (*Dll4*^{flox}*;Nfat-Cre*) (**g,g′**) and *Notch1*$^{flox/flox}$*;Nfatc1pan-Cre/+* (*Notch1*^{flox}*;Nfat-Cre*) sections (**h,h′**).

Arrowheads, endocardium; arrows, trabecular myocardium. Yellow bars, compact myocardium thickness. In **b–d′**,**e–h′** nuclei are DAPI-counterstained. Scale bars, 100 μm. (**i**) Quantification of compact myocardium thickness and trabecular length at E9.5. Data are mean ± s.d. (n = 12 sections from 3 WT and n = 12 sections from 3 mutant embryos of each genotype, ***P < 0.001, by Student's t-test). (**j**) Chart showing the total number of differentially expressed genes identified by RNA-seq (P < 0.05) in the indicated genotypes. Numbers in the green and blue sections indicate upregulated and downregulated genes, respectively. (**k**) Venn diagram representation of the comparative analysis of deregulated genes in the three genotypes. Numbers in black indicate the total number of genes common to at least two genotypes. (**l**) Circular plot of 257 differentially expressed genes, simultaneously presenting a detailed view of the relationships between expression changes (left semicircle perimeter) and processes (right semicircle perimeter). In the left semicircle perimeter, the inner ring represents *Notch1^{flox};Nfat-Cre* data, the middle ring *Dll4^{flox};Nfat-Cre* data and the outer ring *Dll4^{flox};Tie2-Cre* data. 28 of the 257 genes are named. Green, upregulated; blue, downregulated; black, unchanged. Details in Supplementary Table 1. (**m–n′**) E9.5 WT (**m,m′**) and *Dll4^{flox};Nfat-Cre* embryos (**n,n′**), BrdU immunostaining. The myocardium is SMA-counterstained (red). Arrowheads, BrdU-positive nuclei. Scale bars, 50 μm. (**o**) BrdU-positive nuclei as a percentage of total nuclei in myocardium and endocardium. Data are mean ± s.d. (n=3 WT and 3 n=mutant embryos, *P < 0.05 by Student's t-test; NS, not significant). (**p–q′**) *Gpr126* ISH in E9.5 WT (**p,p′**) and *Dll4^{flox};Nfat-Cre* hearts (**q,q′**). Scale bars, 100 μm. Source data are available in Supplementary Table 4. avc, atrio-ventricular canal; la, left atrium; lv, left ventricle; ra, right atrium; rv, right ventricle; myoc, myocardium; endoc, endocardium.

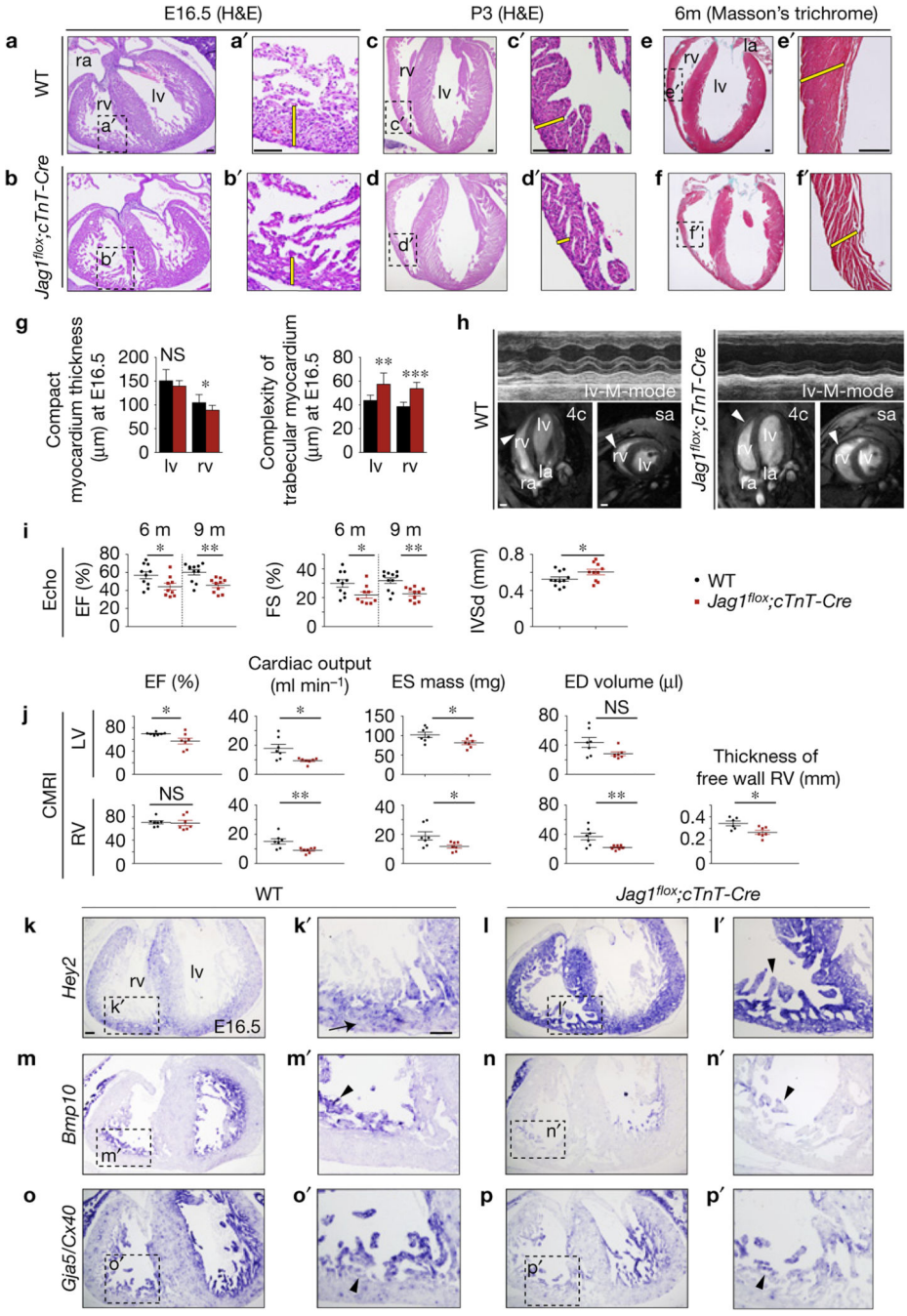

Figure 2.

Myocardial *Jag1* inactivation disrupts chamber maturation and leads to cardiomyopathy and systolic dysfunction. (**a–d′**) Haematoxylin–eosin (H&E) staining of heart sections from WT and *Jag1*$^{flox/flox}$*;cTnT-Cre/+* (*Jag1*^{flox}*;cTnT-Cre*) E16.5 embryos (**a–b′**) and postnatal day 3 (P3) neonates (**c–d′**). (**e–f′**) Masson's trichome staining in 6-month-old hearts. The yellow bars in **a′–f′** indicate compact myocardium thickness. Abbreviations as in Fig. 1. Scale bars, 100 µm. (**g**) Quantification of compact myocardium thickness and trabecular complexity in E16.5 WT, *Jag1*^{flox}*;cTnT-Cre* embryos. Data are mean ± s.d. (*n* = 16 sections from 4 WT

and $n = 16$ sections from 4 mutant embryos, $*P < 0.05$, $**P < 0.01$, $***P < 0.001$, by Student's *t*-test; NS, not significant). (**h**) Echocardiography and CMRI analysis of adult WT and *Jag1^{flox};cTnT-Cre* mice. Left: top, M-mode views of the left ventricle (lv) of a 6-month-old WT mouse. Bottom, CMRI analysis of a 6-month-old WT mouse. Images show four-chamber (4c) and short-axis (sa) views. Arrowheads mark the ventricular wall. Right: top, M-mode views of the left ventricle of a 6-month-old *Jag1^{flox};cTnT-Cre* mouse. Bottom, CMRI analysis of a 6-month-old mutant mouse. Arrowheads mark the thin ventricular wall. Scale bars, 2 mm. (**i**) Echocardiography analysis of left ventricular ejection fraction (EF) and fractional shortening (FS) measured at 6 and 9 months and diastolic interventricular septal wall thickness (IVSd) in WT and *Jag1^{flox};cTnT-Cre* mice. Data are mean ± s.d. ($n = 10$ WT and $n = 9$ mutants at 6 months and $n = 11$ WT and $n = 10$ mutants at 9 months, $*P < 0.05$ and $**P < 0.01$ by Student's *t*-test). (**j**) CMRI analysis of physiological and morphometric parameters in the left (LV) and right ventricles (RV) of 6-month-old WT and *Jag1^{flox};cTnT-Cre* mice. EF, ejection fraction; ES mass, end-systolic mass; ED volume, end-diastolic volume. Data are mean ± s.e.m. ($n = 7$ WT and $n = 7$ mutants, $*P < 0.05$ and $**P <0.01$ by Student's *t*-test; NS,=not significant). (**k–p′**) ISH in E16.5 WT and *Jag1^{flox};cTnT-Cre* heart sections. (**k–l′**) *Hey2* expressed in compact myocardium (**k′**, arrow) is expanded to trabeculae in mutants (**l′**, arrowhead). (**m–n′**) *Bmp10*. (**o–p′**) *Cx40*. Arrowheads in **m′,n′,o′,p′** indicate trabecular myocardium. Scale bars, 100 μm. Source data are available in Supplementary Table 4.

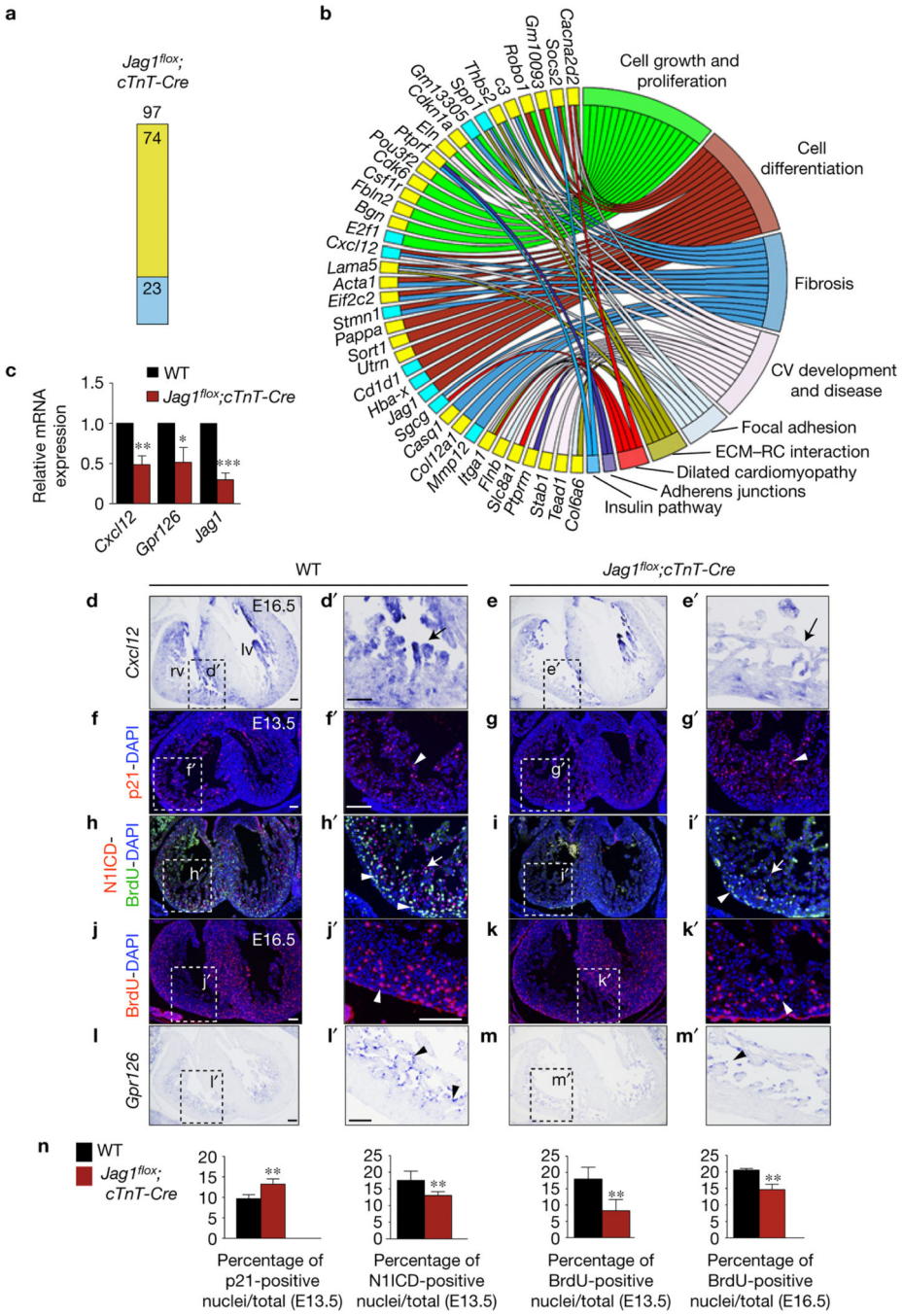

Figure 3.

Jag1 gene profiling and validation. (**a**) Chart showing the number of deregulated genes identified by RNA-seq ($P < 0.05$) in *Jag1*^{flox}*;cTnT-Cre* hearts. Yellow, upregulated; blue, downregulated. (**b**) Circular plot showing 39 representative differentially expressed genes from a total of 97 genes belonging to selected functional categories. Code colour as in **a**. The total number of deregulated genes and the genes represented in the circular plot can be found in Supplementary Table 1. (**c**) qRT–PCR analysis of *Cxcl12, Gpr126* and *Jag1* (as control) in E16.5 WT and mutant ventricles. Data are means ± s.d. ($n = 3$ pools of 3 WT

ventricles per pool and $n = 3$ pools of 3 mutant ventricles per pool; $^{*}P < 0.05$, $^{**}P < 0.01$, $^{***}P < 0.001$ by Student's *t*-test). (**d–e′**) ISH of *Cxcl12* in E16.5 WT and *Jag1*^{flox}*;cTnT-Cre* hearts. Arrows point to myocardial expression. (**f–i′**) Immunostaining for p21 (red nuclei; arrowheads in **f′,g′**), N1ICD (red nuclei; arrowheads in **h′,i′**) and incorporated BrdU (green nuclei; arrows in **h′,i′**) in E13.5 WT and *Jag1*^{flox}*;cTnT* hearts. (**j–k′**) Immunostaining of incorporated BrdU in E16.5 WT (**j,j′**) and *Jag1*^{flox}*;cTnT-Cre* heart sections (**k,k′**). Arrowheads indicate BrdU-positive nuclei (red). (**l–m′**) ISH of *Gpr126* in E16.5 WT and *Jag1*^{flox}*;cTnT-Cre* hearts. Arrowheads indicate endocardial expression. (**n**) Quantification of p21-, N1ICD- and BrdU-positive nuclei in E13.5 and E16.5 *Jag1*^{flox}*;cTnT* ventricles. Data are mean ± s.d. ($n = 6$ WT and 6 mutant embryos, except for E16.5 BrdU quantification, where $n = 3$ WT and $n = 3$ mutant embryos; $^{*}P < 0.01$, by Student's *t*-test). Abbreviations as in Fig. 2. Scale bars, 100 μm. Source data are available in Supplementary Table 4.

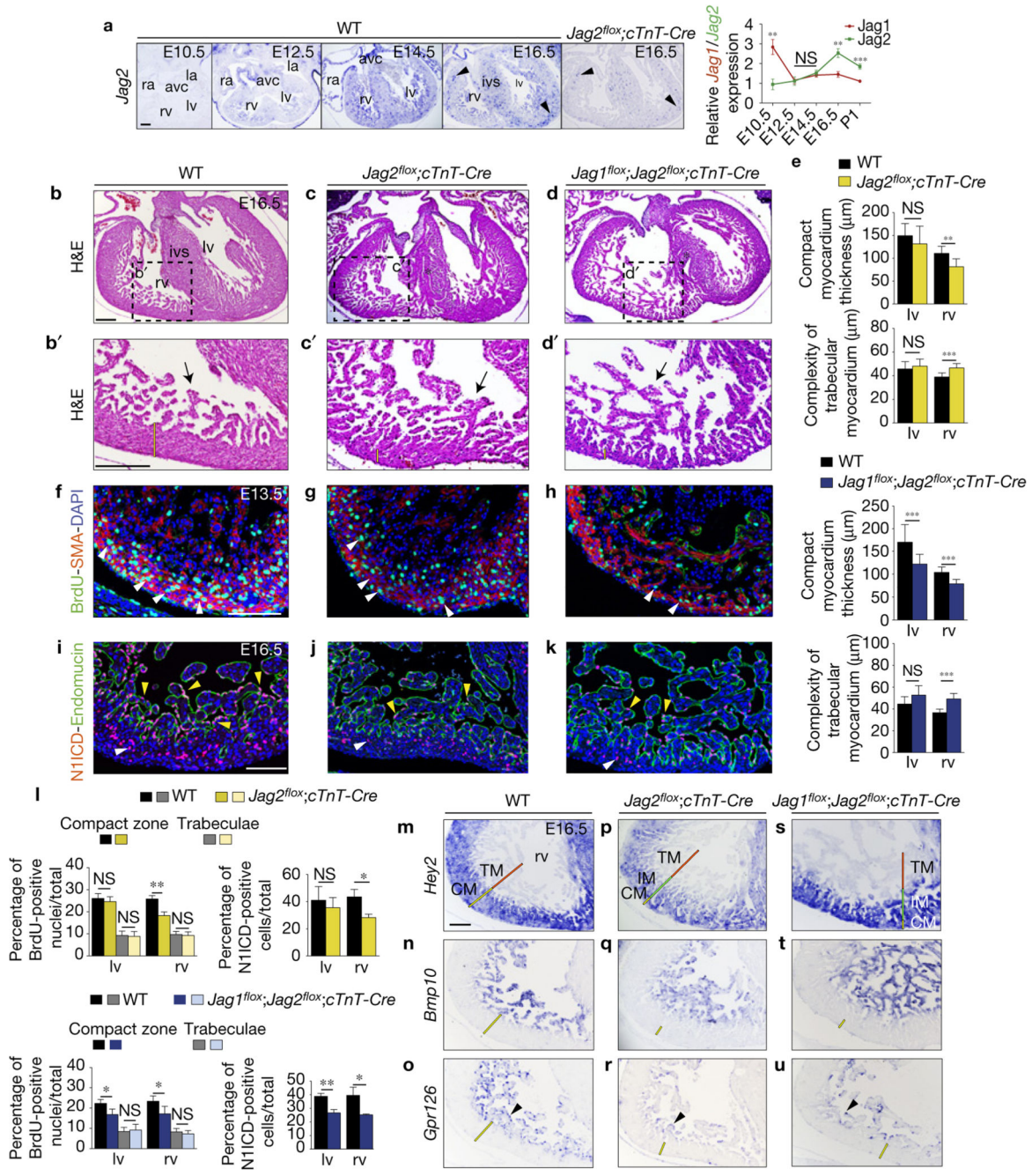

Figure 4.

Myocardial Jag2, together with Jag1, is required for ventricular maturation and compaction. (**a**) ISH of *Jag2* in heart sections from E10.5, E12.5, E14.5, E16.5 WT and E16.5 *Jag2*$^{flox/flox}$;*cTnT-Cre*/+ (*Jag2*^{flox};*cTnT-Cre*) embryos. Abbreviations as in Fig. 1. *cTnT-Cre*-mediated deletion abrogates *Jag2* expression in the myocardium but does not affect expression in coronary vessels (arrowheads). Chart shows relative ratios of *Jag1* and *Jag2* gene expression measured by qRT–PCR. Data are means ± s.d. (n=3 pools of 3 WT ventricles per pool for each stage analysed; $^{**}P < 0.01$, $^{***}P < 0.001$, by Student's t-test; NS, not significant). (**b–d′**) H&E staining of E16.5 WT, *Jag2*^{flox};*cTnT-Cre* and

Jag1^{flox};*Jag2*^{flox};*cTnT-Cre* hearts. The yellow bar in **b′–d′** indicates the thickness of compact myocardium and the asterisk in **c,d** the defective ventricular septum. ivs, interventricular septum. (**e**) Chart showing quantification of compact myocardium thickness and complexity of trabecular myocardium in *Jag2*^{flox};*cTnT-Cre* and *Jag1*^{flox};*Jag2*^{flox};*cTnT-Cre* hearts. Data are mean ± s.d. (n = 9 sections from 3 WT and n = 9 sections from 3 *Jag2*^{flox};*cTnT-Cre*; n = 12 sections from 4 WT and n = 12 sections from 4 *Jag1*^{flox};*Jag2*^{flox};*cTnT-Cre* embryos; $^{**}P < 0.01$, $^{***}P < 0.001$, determined by Student's t-test; NS, not significant). (**f–h**) BrdU (green) and SMA (red) immunostaining in E13.5 WT (**f**), *Jag2*^{flox};*cTnT-Cre* (**g**) and *Jag1*^{flox};*Jag2*^{flox};*cTnT-Cre* hearts (**h**). Nuclei are counterstained with DAPI (blue). (**i–k**) N1ICD immunostaining. In the E16.5 WT heart (**i**), N1ICD (red) labels endocardial nuclei (yellow arrowheads) delineated by endomucin staining (green), and coronary vessels (white arrowheads). *Jag2*^{flox};*cTnT-Cre* (**j**) and *Jag1*^{flox};*Jag2*^{flox};*cTnT-Cre* hearts (**k**) show below-normal N1ICD expression. (**l**) Quantification of BrdU- and N1ICD-positive cells in both genotypes. Data are mean ± s.d. (n = 3 WT and n = 3 *Jag2*^{flox};*cTnT-Cre* for BrdU and N1ICD stainings; n = 3 WT and n=4 *Jag1*^{flox};*Jag2*^{flox};*cTnT-Cre* embryos for BrdU and N1ICD analyses; $^{*}P < 0.05$, $^{**}P < 0.01$, by Student's t-test; NS, not significant). (**m–u**) ISH analysis. *Hey2* marks compact myocardium (CM, yellow bar) in **m,p,s**. The red and green bars in **p,s** mark the trabecular (TM) and intermediate myocardium (IM) respectively. *Bmp10* labels TM in WT (**n**), *Jag2*^{flox};*cTnT-Cre* (**q**) and *Jag1*^{flox};*Jag2*^{flox};*cTnT-Cre* ventricles (**t**). (**o,r,u**) *Gpr126* transcription. rv, right ventricle. Scale bars, 100 μm. Source data are available in Supplementary Table 4.

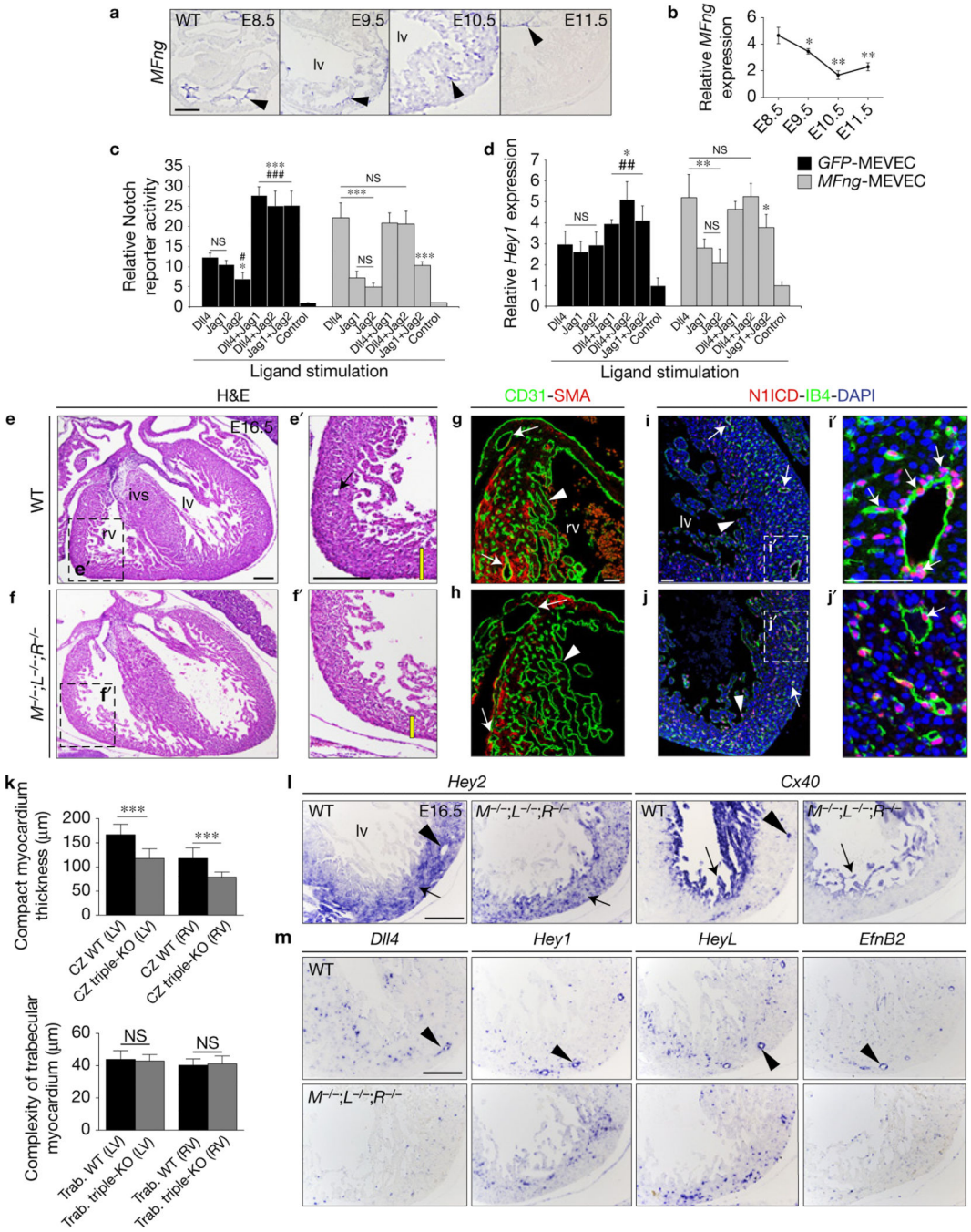

Figure 5.

MFng modulates Notch selectivity towards its ligands and systemic *Fng* abrogation disrupts coronary vessel development. (**a**) ISH analysis of *MFng*. Arrowheads point to expression in chamber endocardium (E8.5–10.5) and avc (E11.5). (**b**) Relative *MFng* expression by qRT–PCR from E8.5–11.5 ventricles. Data are means ± s.d. ($n = 3$ pools of 5 WT hearts at E8.5, and $n = 3$ pools of 3 ventricles per pool at E9.5–11.5, $^{*}P < 0.05$, $^{**}P < 0.01$, by Student's *t*-test). (**c**) Notch signalling activity measured by 10xCBF1–Luc reporter assay in MEVEC infected with control GFP lentivirus (*GFP*-MEVEC, black bars) or with a MFng lentivirus

(*MFng*-MEVEC, grey bars) and stimulated with immobilized Notch ligands. Control represents the activity of the Notch reporter in non-stimulated MEVEC. (**d**) qRT–PCR analysis of *Hey1* expression in *GFP*-MEVEC (black bars) or *MFng*-MEVEC (grey bars). Symbols: *, significant difference compared with Dll4; #, compared with Jag1. Data are mean ± s.d. ($n = 4$ independent biological replicates for each condition in **c**, and $n = 3$ for each condition in **d**; *, #$P < 0.05$, ## $P < 0.01$, ***, ### $P < 0.001$ by Student's *t*-test; NS, not significant). These data are representative of 3 independent experiments. (**e–f′**) H&E staining of E16.5 WT (**e,e′**) and *M;L;RFng*-deficient hearts ($M^{-/-};L^{-/-};R^{-/-}$ **f,f′**). The yellow bar in **e′,f′** indicates the thickness of compact myocardium and the arrow in **e′** points to a coronary vessel. (**g,h**) WT (**g**) and $M^{-/-};L^{-/-};R^{-/-}$ (**h**) ventricular sections stained with SMA (myocardium, red) and CD31 (Pecam1) (green), which labels the endocardium (arrowheads) and the endothelium of coronary vessels (arrows). (**i–j′**) N1ICD (red) stains chamber endocardium (**i,j**, arrowheads) and coronary vessels (**i′–j′**, arrows), co-stained with isolectin B4 (IB4, green). Nuclei are counterstained with DAPI (blue). (**k**) Quantification of compact myocardium thickness (CZ, myocardial compact zone) and trabecular myocardium complexity in E16.5 $M^{-/-};L^{-/-};R^{-/-}$ mice. Data are mean ± s.d. ($n = 3$ WT and $n = 3$ triple mutant embryos, ***$P < 0.001$, by Student's *t*-test; NS, not significant). (**l,m**) ISH analysis of *Hey2* and *Cx40* (**l**) and *Dll4*, *Hey1*, *HeyL* and *EfnB2* (**m**) expression in WT and $M^{-/-};L^{-/-};R^{-/-}$ mice. Scale bars, 100 μm, except in **g–j′** where scale bars are 50 μm. Source data are available in Supplementary Table 4.

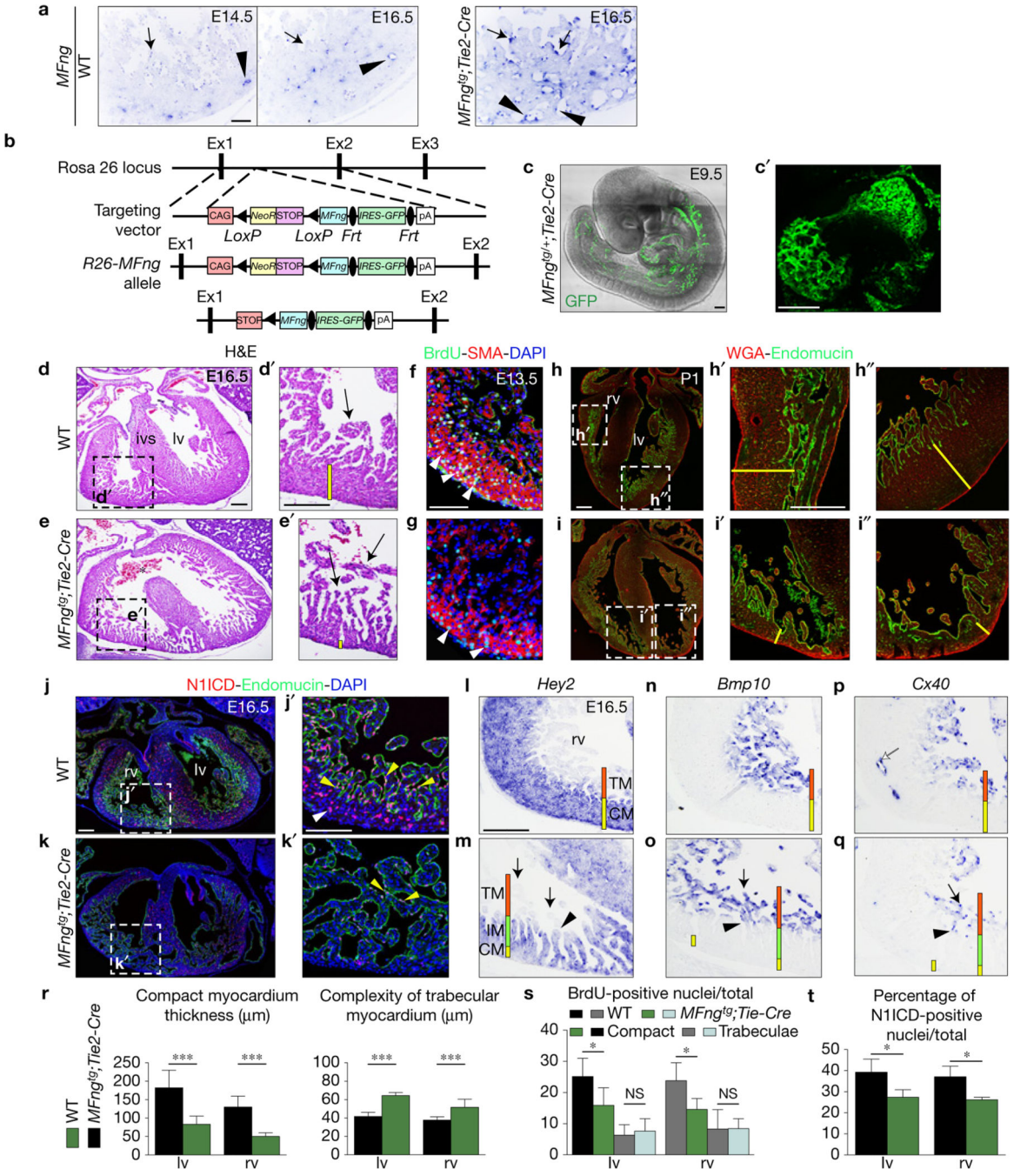

Figure 6.

Forced *MFng* expression in the endocardium disrupts chamber development. (**a**) ISH showing *MFng* expression in coronary vessel endothelium (arrowheads) but not in endocardium (arrows) of E14.5–16.5 WT embryos, and ectopic *MFng* expression in endocardium (arrows) and in coronary vessels endothelium (arrowheads) of $MFng^{tg}$;*Tie2-Cre* embryos. (**b**) Gene targeting strategy used to generate the conditional $MFng^{tg}$ line. (**c**) Whole-mount two-photon microscopy image of an E9.5 $MFng^{tg/+}$;*Tie2-Cre/+* embryo. (**c′**) Heart detail showing transgenic expression. (**d–e′**) H&E staining of E16.5 WT and

MFng$^{tg/tg}$*;Tie2-Cre/+* (*MFng*^{tg}*;Tie2-Cre*) ventricles. *MFng*^{tg}*;Tie2-Cre* hearts show defective ventricular septum (**e**, asterisk). The yellow bar in **d′,e′** marks the thickness of compact myocardium. (**f,g**) BrdU (green) and SMA (red) staining in E13.5 WT (**f**) and *MFng*^{tg}*;Tie2-Cre* hearts (**g**). Nuclei are counterstained with DAPI (blue). (**h–i″**) Postnatal day 1 (P1) heart stained with wheat-germ agglutinin (WGA) and endomucin. The yellow bar in **h′-i″** marks the thickness of compact myocardium. (**j–k′**) General view of the E16.5 WT (**j**) and *MFng*^{tg}*;Tie2-Cre* hearts (**k**) stained for N1ICD and endomucin. N1ICD is expressed in WT endocardium (**j′**, yellow arrowheads) and coronaries (**j′**, white arrowhead) and very attenuated in the transgenic heart (**k′**). (**l–q**) ISH. *Hey2* expression reveals a thick compact myocardium in the E16.5 WT heart (**l**) and a very thin and disorganized counterpart in the *MFng*^{tg}*;Tie2-Cre* heart (**m**). *Bmp10* and *Cx40* label ventricular trabeculae in WT embryos (**n,p**) and both are expressed at the distal tip of trabeculae in *MFng*^{tg}*;Tie2-Cre* embryos (**o,q**, arrows). *Cx40* is also expressed in WT coronaries (**p**, white arrow) but not in transgenic embryos (**q**). The arrowhead (**m,o,q**) marks the transition between *Bmp10*$^{-}$,*Cx40*$^{-}$ and *Bmp10*$^{+}$,*Cx40*$^{+}$ trabeculae. The red and yellow bars (**l–q**) mark the trabecular (TM) and compact myocardium (CM) and the green bar (**m,o,q**) marks the intermediate (IM) myocardium. Scale bars, 100 μm except in **b,b′**, where bars, 50 μm. (**r**) Quantification of ventricular morphological parameters of E16.5 WT ($n = 3$) and *MFng*^{tg}*;Tie2-Cre* ($n = 4$) embryos. (**s**) BrdU-positive nuclei/total in E13.5 WT and *MFng*^{tg}*;Tie2-Cre* hearts ($n = 3$ WT and $n = 3$ transgenic). (**t**) Quantification of N1ICD-positive nuclei in E16.5 WT ($n = 3$) and transgenic ($n = 3$) hearts. Data are mean ± s.d. $^{*}P < 0.05$, $^{***}P < 0.001$, by Student's *t*-test; NS, not significant. Source data are available in Supplementary Table 4.

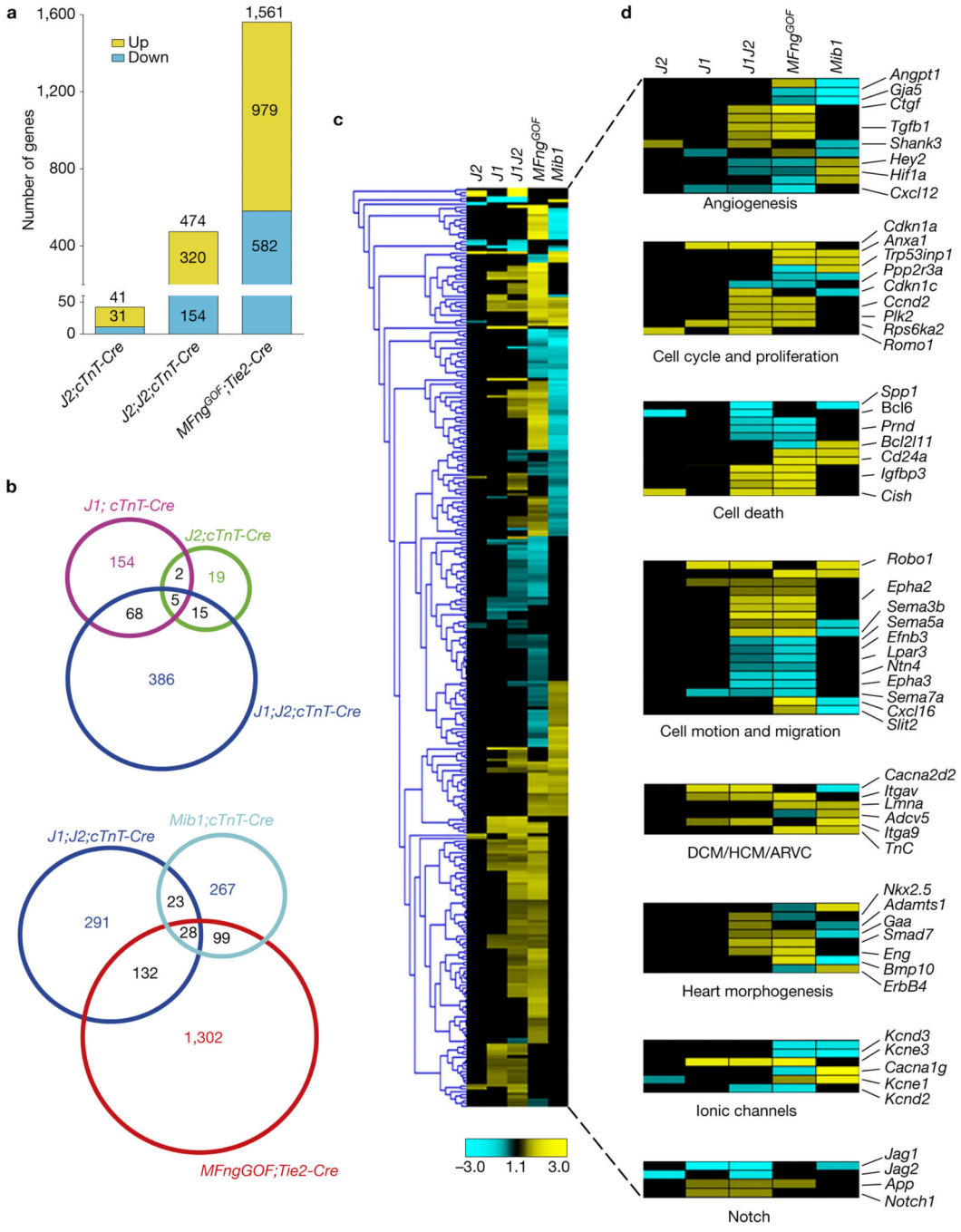

Figure 7.

Comparative expression profiling of *Jag2*^{flox}*;cTnT-Cre*, *Jag1*^{flox}*;cTnT-Cre*, *Jag1*^{flox}*;Jag2*^{flox}*;cTnT-Cre*, *MFng*^{GOF}*;Tie2-Cre* (*MFng*^{tg}*;Tie2-Cre*) and *Mib1*^{flox}*;cTnT-Cre* mutants. GOF, gain of function. (**a**) Chart indicating the total number of deregulated genes identified by RNA-seq ($P < 0.05$) in E15.5 *Jag2*^{flox}*;cTnT-Cre* mutants (*J2;cTnT-Cre*), *Jag1*^{flox}*;Jag2*^{flox}*;cTnT-Cre* mutants (*J1;J2;cTnT-Cre*) and *MFng*^{GOF}*;Tie2-Cre* transgenic embryos (*MFng*^{GOF}*;Tie2-Cre*). The total number of differentially expressed genes per genotype is indicated at the top of every column. Numbers in the yellow section indicate

upregulated genes; numbers in the blue section indicate downregulated genes. (**b**) Venn diagram representation of the comparative analysis of the deregulated genes in the five genotypes analysed (*Jag1*^{flox}*;cTnT-Cre*, *Jag2*^{flox}*;cTnT-Cre*, *Jag1*^{flox}*;Jag2*^{flox}*;cTnT-Cre*, *MFng*^{GOF}*;Tie2-Cre* and *Mib1*^{flox}*;cTnT-Cre*). Top, comparison of *J1* and *J2* single and *J1;J2;cTnT-Cre* double mutants. Bottom, comparison of *J1;J2;cTnT-Cre*, *Mib1;cTnT-Cre* and *MFngGOF;Tie2-Cre* embryos. Numbers in black indicate the total number of genes common to at least two genotypes. (**c**) Heat map representation of the 372 genes differentially expressed in at least two of the five mutant genotypes. Yellow, upregulated; blue, downregulated; black, not significant change. (**d**) Subsets of genes clustered into functional classes (right panels). The total number of deregulated genes for each genotype and the genes represented in the heat map can be found in Supplementary Table 1.

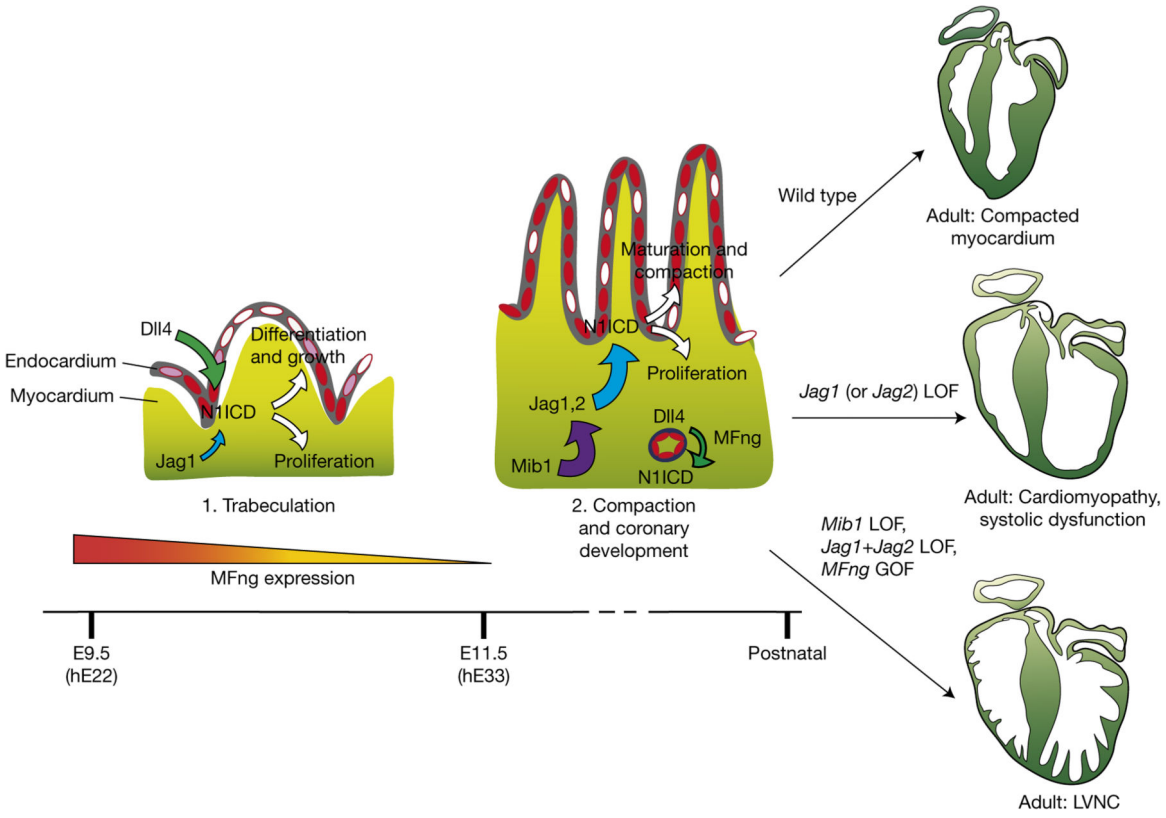

Figure 8.

Sequential Notch ligand–receptor activation during ventricular chamber development. In the early ventricle (1) endocardial Dll4 and myocardial Jag1 can activate Notch1 in the endocardium. Expression of MFng in the endocardium favours Dll4 signalling to Notch1 (large green arrow) and Jag1 signalling is low (small blue arrow). Notch1 activation (red) promotes cardiomyocyte proliferation, trabecular growth and patterning. As chamber development proceeds (2), endocardial MFng expression reduces progressively (similarly to Dll4) allowing myocardial Jag1 to activate Notch1 in the myocardium. Jag2 expression is progressively upregulated in chamber myocardium, where it acts together with Jag1 to promote chamber proliferation, patterning and trabecular compaction to give rise to the functional ventricular wall (large blue arrow). At this time, MFng and Dll4 are required for Notch1 activation in coronary vessels (small green arrow). Inactivation of *Jag1* (or *Jag2*) in the myocardium disrupts chamber maturation and leads to cardiomyopathy. Mib1 acts upstream of Jag1 and Jag2 in this process: *Mib1* inactivation in the myocardium causes LVNC. A similar phenotype is produced when both *Jag1* and *Jag2* are deleted in the myocardium and when *MFng* is constitutively expressed in the endocardium (presumably causing persistent inhibition of Jag1 and Jag2 signalling). LOF, loss of function.